

Single-seed generation of Brownian paths and integrals for adaptive and high order SDE solvers

Andraž Jelinčič

Department of Mathematical Sciences

University of Bath, UK

{aj2382, jmf68}@bath.ac.uk

James Foster

Patrick Kidger

Cradle.bio

Zurich, Switzerland

math@kidger.site

May 28, 2024

Abstract

Despite the success of adaptive time-stepping in ODE simulation, it has so far seen few applications for Stochastic Differential Equations (SDEs). To simulate SDEs adaptively, methods such as the Virtual Brownian Tree (VBT) have been developed, which can generate Brownian motion (BM) non-chronologically. However, in most applications, knowing only the values of Brownian motion is not enough to achieve a high order of convergence; for that, we must compute time-integrals of BM such as $\int_s^t W_r dr$. With the aim of using high order SDE solvers adaptively, we extend the VBT to generate these integrals of BM in addition to the Brownian increments. A JAX-based implementation of our construction is included in the popular Diffraction library (github.com/patrick-kidger/diffrax).

Since the entire Brownian path produced by VBT is uniquely determined by a single PRNG seed, previously generated samples need not be stored, which results in a constant memory footprint and enables experiment repeatability and strong error estimation. Based on binary search, the VBT's time complexity is logarithmic in the tolerance parameter ε . Unlike the original VBT algorithm, which was only precise at some dyadic times, we prove that our construction exactly matches the joint distribution of the Brownian motion and its time integrals at any query times, provided they are at least ε apart.

We present two applications of adaptive high order solvers enabled by our new VBT. Using adaptive solvers to simulate a high-volatility CIR model, we achieve more than twice the convergence order of constant stepping. We apply an adaptive third order underdamped or kinetic Langevin solver to an MCMC problem, where our approach outperforms the No U-Turn Sampler, while using only a tenth of its function evaluations.

1 Introduction

In this paper, we introduce a method for simulating Brownian motion (BM) which can power both adaptive time-stepping and high order numerical solvers for Stochastic Differential Equations (SDEs). The former needs the ability to query the Brownian path non-chronologically, and the latter requires access to integrals of BM, also known as “Lévy areas” (see Definition 2.2). The capability to combine these is new here.

Rössler [Röß10] proposed a solver for additive-noise SDEs which achieves strong order $3/2$ (see Definition 2.1), provided access to space-time Lévy area (see Definition 2.2). In [FLO21] Foster found a solver for the underdamped (also known as kinetic) Langevin diffusion with strong order 3, provided access to space-time-time Lévy area (Definition 2.2). The aim of this paper is to enable these high order solvers to be used adaptively, which requires a new method of simulating Brownian motion and its Lévy areas.

Although adaptive solvers such as Dormand–Prince 5(4) [DP80] are widely used in ODE simulation [BHB04], applying them to SDEs [GL97; IJE15] is more challenging and far less common. To see why, consider the usual way to generate a BM W by drawing independent Gaussian random variables $N(0, h)$ for each increment $W_{t+h} - W_t$. When an adaptive solver’s internal error estimate is too large, it backtracks and redoes the last step but with a smaller step size $h' < h$. Since the error estimate depends on the value of $W_{t+h} - W_t$, it cannot be discarded, but the new sample $W_{t+h'}$ must be conditioned on W_{t+h} . This backtracking sometimes needs to be repeated several times. To facilitate this, non-chronological BM generators have been developed [RN17; Kid+21a]. One of these is the Virtual Brownian Tree (VBT) [Li+20], on which our method is based.

Most methods of generating Brownian motion are query-dependent, meaning that the generated Brownian path depends both on the random seed, and the query times $s, t \in \mathbb{R}$ at which $W_t - W_s$ is evaluated. With the VBT, however, the initial random seed completely determines the entire Brownian path. This has the downside of requiring a pre-specified tolerance parameter ε and having an $\mathcal{O}(\log \varepsilon)$ time complexity per evaluation (see Section 2.1). However, it brings several benefits, including an $\mathcal{O}(1)$ memory cost, easier experiment repeatability, straightforward computation of solver orders, and a concise proof of correctness.

To use the aforementioned SDE solvers adaptively, we extend the VBT to additionally generate the space-time and space-time-time Lévy areas of BM. Like the VBT, our approach is query-independent and has the same computational complexity. In Theorems 3.7 and 4.2 we show that our construction exactly matches the joint distribution of the Brownian increments and Lévy areas for all query points separated by at least ε . For contrast, the original VBT was precise only at dyadic query times and only generated Brownian increments. Our implementation is available as part of the software package *DiffraX* (github.com/patrick-kidger/diffrax).

1.1 Structure of this paper

Section 2 introduces key terminology and related work, with a detailed explanation of VBT in Section 2.1.

In Section 3.1 we present our new mathematically-precise interpolation method for the Brownian-increments-only case of VBT and prove that it produces correctly distributed samples also at non-dyadic times. The rest of Section 3 contains the theoretical results required to generate the space-time Lévy area H and space-time-time Lévy area K adaptively. Section 3.2 gives a new version of Chen’s relation for the triple (W, H, K) . Section 3.3 gives the rule for generating these at dyadic points which is then extended to non-dyadic times in Section 3.4.

In Section 4, we condense this theory into an improved algorithm for the VBT. In addition to augmenting the VBT with Lévy areas, we introduce a further improvement called “Interval Normalisation” (see Section 4.1), which substantially reduces numerical errors. In Section 4.3 we prove that given a mild assumption on the spacing of query points, our construction exactly matches the full pathwise joint distribution of the BM and its Lévy areas.

In Section 5 we present two applications of the new VBT algorithm, first to the Cox-Ingersoll-Ross model, which is provably difficult to solve with constant step sizes, and second to an MCMC sampling problem, where we demonstrate the performance of the third order Langevin solver when used adaptively.

2 Related Work and Theoretical Background

SDE simulation Suppose the task is to simulate an SDE of the form

$$dX_t = f(X_t)dt + \sum_{i=1}^d g_i(X_t)dW_t^{(i)}, \quad X_0 = x_0,$$

where the solution $X = (X_t)_{t \in [0, T]}$ takes values in \mathbb{R}^e , $W = (W^{(1)}, \dots, W^{(d)})$ denotes a standard d -dimensional Brownian motion (BM) and $f, g_i : \mathbb{R}^e \rightarrow \mathbb{R}^e$ are suitably regular vector fields. SDE simulation comes in two flavors: weak and strong. In the former, we are interested in distributional properties of the random variable X_t , such as its moments; whereas in the case of strong simulation, we are given a particular path of the BM $w : [0, T] \rightarrow \mathbb{R}^d$ and the aim is to generate a sample path $\hat{X}(w) = (\hat{X}_t(w))_{t \in [0, T]}$ which satisfies the SDE together with w . An important measure of success for an SDE solver is its strong order of convergence (SOC).

Definition 2.1 (Strong order of convergence (SOC)). Suppose we have a strong SDE solver, which given a Brownian path w produces a solution $\hat{X}_N(w)$ using N computational steps. Let $X(w)$ be a true solution of the SDE corresponding to w (usually obtained via a numerical solver very small steps). Then the strong error of the solver is

$$\epsilon_{\text{strong}}(N) := \sup_{0 \leq n \leq N} \mathbb{E}_w \left[\left| \hat{X}_N(w)_{t_n} - X(w)_{t_n} \right|^2 \right]^{\frac{1}{2}}.$$

The solver has a SOC γ if there exists a constant $C > 0$ s.t. $\epsilon_{\text{strong}}(N) \leq C \left(\frac{T}{N}\right)^\gamma \quad \forall N \in \mathbb{N}$. When using a constant-step solver $h = \frac{T}{N}$ is just the step size, whereas in adaptive solvers it is the mean step size.

A more in-depth introduction to SDE simulation can be found in [HK21].

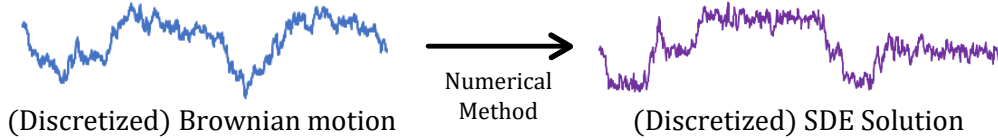


Figure 1: An SDE solver is a deterministic function from a Brownian path to an SDE trajectory [Fos23].

Depending on the SDE being simulated, a solver may need access to certain ‘‘Levy areas’’ in order to achieve a high SOC.

Definition 2.2 (Brownian bridge and Lévy areas). Let $0 \leq s \leq r \leq t$ and let $W : [0, \infty) \rightarrow \mathbb{R}^d$ be a Brownian motion. Write $W_{s,t} = W_t - W_s$. Then the Brownian bridge on $[s, t]$ evaluated at r is given by

$$B_r^{s,t} := \mathbb{E}[W_r \mid W_s = W_t = 0] = W_{s,r} - \frac{r-s}{t-s}W_{s,t} \quad \text{with convention that when } s = t, \quad B_s^{s,s} := 0.$$

We define the ‘‘space-space Lévy area’’ $A_{s,t} \in \mathbb{R}^{d \times d}$ (usually called just ‘‘Lévy area’’) as

$$A_{s,t}^{(i,j)} := \frac{1}{2} \left(\int_s^t W_{s,r}^{(i)} dW_r^{(j)} - \int_s^t W_{s,r}^{(j)} dW_r^{(i)} \right), \quad \text{for } i, j \in \{1, \dots, d\},$$

the ‘‘space-time Lévy area’’ $H_{s,t} \in \mathbb{R}^d$ as

$$H_{s,t} := \frac{1}{t-s} \int_s^t B_r^{s,t} dr, \quad \text{and}$$

and the ‘‘space-time-time Lévy area’’ $K_{s,t} \in \mathbb{R}^d$ as

$$K_{s,t} := \frac{1}{(t-s)^2} \int_s^t B_r^{s,t} \left(\frac{t+s}{2} - r \right) dr.$$

For general multidimensional SDEs, a solver without access to space-space Lévy area A can attain a SOC of at most $\gamma = \frac{1}{2}$ [CC80]. Unfortunately, space-space Lévy area is not Gaussian and notoriously difficult to sample from. Approximations to Lévy area have been well studied (see [Dav14; Dic07; Jel+23; KPW92; Fos20; FH22; MR22; Wik01]), and the only method of generating space-space Lévy area with SOC higher than $\frac{1}{2}$ is that by [GL94], which only applies when $d = 2$.

High order solvers with space-time Lévy area For certain classes of SDEs, a high SOC can be achieved even with access to only space-time Lévy area H , which is Gaussian and hence easier to sample than space-space Lévy area A . In particular [Röß10] proposes a solver using space-time Lévy area with a SOC of 1.5 when applied to additive-noise SDEs, that is when g has no dependence on X_t and can be written as just $g(t)$. [FRS23] extended this to a more general class of SDEs called commutative noise SDEs, in which the diffusion vector field g commutes in the Lie bracket (i.e. the columns satisfy $g'_i g_j = g_i g'_j$).

Another class of SDEs that admit high order solvers are the Langevin diffusions, which originate from molecular dynamics [LG97], but are now commonly used in Markov Chain Monte Carlo applications [Bro+11; Li+19]. While access to space-time Lévy area enables solvers to achieve SOC 2, it is possible to achieve even SOC 3 if the solver also uses space-time-time Lévy area (which is also Gaussian and easy to generate) [FLO21].

Adaptive time-stepping is a widely used technique in ODE simulation [Söd02; HNW93]. It involves numerically estimating the error of the solver at every step of the solution, and decreasing the step size when errors are too large, or increasing when they are small. However, for SDEs, constant time-stepping is still the predominant paradigm, despite the fact that some problems, such as simulating the CIR model, provably cannot be solved efficiently with constant steps [HJ19].

The first significant attempt at adaptive stepping for SDE simulation is by [GL97], where steps of the solver can be halved if large numerical errors are detected. To enable this, the authors proposed an early iteration of the Brownian Tree, which only supported dyadic time-step refinements and required keeping the results of previous queries in memory.

More advanced step-size controllers, such as the PID controller [Söd03; HW02; HNW08], can also be used for SDE simulation [IJE15]. However, to facilitate that, the BM generation method must also accept queries at non-dyadic times (i.e. instead of always just halving or doubling the step, we permit an arbitrary step size), so methods such as the Brownian Interval by [Kid+21a] and Rejection Sampling with Memory (RSwM) by [RN17] were proposed. These are unfortunately query dependent, and require storing previously drawn samples in memory. To address this issue [Li+20] proposed the Virtual Brownian Tree, which is query-independent and has a constant memory cost, but is imprecise at non-dyadic points, due to its use of piecewise-constant interpolation. Our new interpolation method proposed in Section 3.1 fixes this and matches the target distribution exactly.

Lévy’s construction The VBT is inspired by Lévy’s construction of Brownian motion, which splits the interval $[0, 1]$ into progressively smaller dyadic sub-intervals. This means that at level d , we have evaluated the BM at all t of the form $k2^{-d}$ with $k \in \{0, 1, \dots, 2^d\}$. As we descend through the levels, this path converges to BM. The way to do this for Brownian increments is well known, and has long been used as a neat proof for the existence of BM. Adding a version of space-time Lévy area to this construction was first discussed by [Mau98; BHB04]. [Fos20] streamlined this construction and found a way to generate space-time-time Lévy area at dyadic points. Here we extend the latter to non-dyadic points, integrate all this into the VBT algorithm and prove the correctness of its output distribution.

2.1 The Virtual Brownian Tree

The Virtual Brownian Tree (VBT), proposed by [Li+20] and inspired by [GL97], represents a deterministic function f_{VBT} from the space of m -bit seeds $\{0, 1\}^m$ to the space of continuous paths $\mathcal{C}([t_0, t_1], \mathbb{R}^d)$. This means that only a single seed needs to be stored to reconstruct the entire path, which reduces the memory

cost to $\mathcal{O}(1)$. Unlike other approaches (Brownian Interval by [Kid+21a] or RSWM by [RN17]), which have to store previous queries, the VBT is stateless. While most methods are concerned with the distribution of each individual sample conditioned on previously generated samples, VBT is concerned with the distribution of the entire path $w: [t_0, t_1] \rightarrow \mathbb{R}^d$. Specifically, if \mathcal{U} is a uniform measure in seed space, then we want the push-forward $\mathcal{U} \circ f_{\text{VBT}}^{-1}$ to be close to the Wiener measure on the space of paths (which can be matched exactly on sufficiently spaced cylinder sets using our new interpolation method proposed in Section 3.1).

Remark 2.3. Note that a continuous random variable cannot be precisely matched by its floating-point computational approximation, which necessarily introduces some discretisation. Here and throughout the paper we neglect this discrepancy.

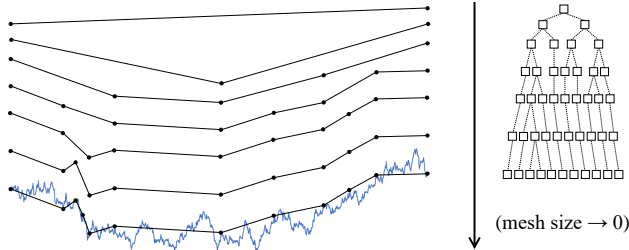


Figure 2: An illustration of the original Brownian Tree by [GL97] (image from [Fos23]).

2.1.1 Splittable PRNGs

The first key ingredient is “splittable” pseudo-random number generator (PRNG) seeds [Sal+11; CP13].

Given an m -bit random seed $\rho \in \{0, 1\}^m$, splitting is an operation that produces some n new m -bit random seeds $\rho_1, \dots, \rho_n \in \{0, 1\}^m$, as a deterministic function of ρ , for which $\rho, \rho_1, \dots, \rho_n$ produce statistically independent streams of random numbers when used as the seed for a PRNG.

Given any rooted tree, we can associate a random seed with every node in the tree in the following way.

Let $(V, E, *)$ be a rooted tree, where V is a vertex set,

$$E \subseteq \{\{x, y\} : x, y \in V, x \neq y\}$$

a corresponding undirected edge set (connected and without cycles), and $* \in V$ denotes the root. For any $x \in V$, let $\Gamma(x) = \{y \in V : \{x, y\} \in E\}$ denote the set of vertices adjacent to x .

Let $\rho \in \{0, 1\}^m$ be an m -bit seed, which we associate with the root $*$. Split ρ into $\rho_1, \dots, \rho_{|\Gamma(*)|}$ random seeds and pair each one with a corresponding element $v_i \in \Gamma(*)$. Recursively split each ρ_i and pair the resulting seeds with the elements of $\Gamma(v_i)$, etc., repeating this procedure throughout the tree.

By fixing a rooted tree $(V, E, *)$ and a root seed ρ , we may deterministically create a PRNG at every node in the tree. Provided we remember only the tree structure and the root seed s , we can later rematerialise every PRNG sequence, for every node of the tree, without holding the samples in memory.

2.1.2 Generating Brownian samples

We generate the value of the Brownian path $w: [t_0, t_1] \rightarrow \mathbb{R}^d$ at a time $r \in [t_0, t_1]$ using a binary-search-like procedure. We start with $s = t_0$, $u = t_1$. In each step we set $t = \frac{s+u}{2}$ and use the values of w_s and w_u to compute w_t using the Brownian bridge function (a special case of Eq. (2)):

$$w_t = \text{bridge}(s, t, u, w_s, w_u, \hat{\rho}) := \frac{w_s + w_u}{2} + \frac{1}{2}\sqrt{u-s}\mathcal{N}(0, \mathbf{I}_d, \hat{\rho}). \quad (1)$$

Here, $\mathcal{N}(\cdot, \cdot, \hat{\rho})$ denotes a Gaussian pseudo-random variable generated using the seed $\hat{\rho}$, which is the PRNG seed corresponding to the current node in the binary search tree (as per Section 2.1.1). To descend into a

child node, we halve the interval by setting either $s \leftarrow t$ or $u \leftarrow t$ such that the query time r remains in $[s, u]$. This is repeated until the size of $[s, u]$ is smaller than the desired tolerance $\varepsilon > 0$.

Let $L = \lceil -\log_2(\varepsilon) \rceil$ and $V = \{t_0 + (t_1 - t_0)k2^{-L} : k \in \{0, 1, \dots, 2^L\}\}$. By recording only the root-level seed $\sigma \in \{0, 1\}^m$, and computing the seeds of child nodes as we descend the tree, the Brownian sample w_v is completely determined for all $v \in V$. The full procedure is given in Algorithm 1.

Algorithm 1 Sampling from the Virtual Brownian Tree using the `VirtualBrownianTree.eval` function. `split_seed` denotes splitting a PRNG seed, and `bridge` denotes the Brownian bridge from Eq. (1).

Input: r - evaluation time, $[t_0, t_1]$ - definition interval, ρ - PRNG seed, d - dimension, ε - tolerance.

Result: Approximation to w_r

```

 $\rho, \hat{\rho} \leftarrow \text{split\_seed}(\rho, 2)$ 
 $s \leftarrow t_0, u \leftarrow t_1$ 
 $w_s \leftarrow 0$ 
 $w_u \leftarrow \mathcal{N}(0, (t_1 - t_0)\mathbf{I}_{d_w}, \hat{\rho})$ 

while  $|u - s| > \varepsilon$  do
   $t \leftarrow (s + u)/2$ 
   $\rho_1, \rho_2, \hat{\rho} \leftarrow \text{split\_seed}(\rho, 3)$  ▷  $\hat{\rho}$  to generate the midpoint, and  $\rho_1, \rho_2$  for children nodes.
   $w_t \leftarrow \text{bridge}(s, t, u, w_s, w_u, \hat{\rho})$ 
  if  $r > t$  then ▷ Descend into the right child.
     $s \leftarrow t, w_s \leftarrow w_t$ 
     $\rho \leftarrow \rho_1$ 
  else ▷ Descend into the left child.
     $u \leftarrow t, w_u \leftarrow w_t$ 
     $\rho \leftarrow \rho_2$ 
  end if
end while
 $w_r \leftarrow \text{final\_interpolation}(s, r, u, w_s, w_u, \rho)$  ▷ Defined below, originally piecewise constant.
return  $w_r$ 

```

The main use case will be to sample a Brownian increment $w(r_1) - w(r_0)$ (when an SDE solver steps from r_0 to r_1). In that case, we separately sample $w(r_0)$ and $w(r_1)$ using Algorithm 1, and then return $w(r_1) - w(r_0)$. While this takes $\mathcal{O}(\log(1/\varepsilon))$ time, it has the advantage that it requires only $\mathcal{O}(1)$ memory.

In the original algorithm, `final_interpolation` was just piecewise constant, but in Section 3.1 we propose an alternative that guarantees the correct distribution at all times, not only at dyadic ones.

2.1.3 The VBT and strong SDE simulation

As long as we use the same seed, the VBT will always generate the same Brownian path, and so all solvers using that Brownian path as input will always follow the same trajectory of the simulated SDE, no matter what step sizes they use. With the usual query-dependent BM generators (where query times can influence the resulting path), this would only be the case if all solvers used exactly the same step sizes.

The usual approach for computing the strong order of an SDE solver is to first generate a very finely discretised Brownian path, store it in memory, and then run the solver using that path. When using GPU acceleration libraries to alleviate the computational cost of strong SDE simulation (e.g. in the case of diffusion models, [Son+21]) the above workflow needs to be parallelised, and hundreds of finely discretised Brownian paths must be stored in video memory simultaneously. By using the VBT one can ensure that all of the solvers being compared will be fed the same Brownian path, no matter at what times they query it, while needing to store just a single 64-bit seed per path. This is especially relevant when evaluating adaptive solvers, for which we cannot pre-specify at which times they will evaluate the Brownian path.

Neural SDEs [Che+18a; Kid+21a; Kid+21b] pose a similar challenge. To train these, the Brownian path used on the forward pass must be evaluated backwards in time. Normally, this requires storing all samples in memory, incurring a significant cost. In addition, when training via “optimise-then-discretise” the backwards pass might query the BM at different times than the forward pass, while requiring the new samples to be conditioned on the samples of the forward pass. Both of these difficulties can be avoided by using the VBT.

3 Exact simulation of Brownian motion and Lévy area

3.1 New interpolation method for Brownian increments

Let ε be the tolerance parameter, $L = \lceil -\log_2(\varepsilon) \rceil$ and $V = \{t_0 + (t_1 - t_0)k2^{-L} : k \in \{0, 1, \dots, 2^L\}\}$. Suppose $w : [t_0, t_1] \rightarrow \mathbb{R}^d$ given by $r \mapsto \text{VirtualBrownianTree.eval}(r, [t_0, t_1], \rho, d, \varepsilon)$ is the path generated by Algorithm 1. By Lévy’s construction of Brownian motion, we have that if the seed ρ was drawn uniformly at random and W is a Brownian motion, then (with $\stackrel{d}{=}$ denoting equality in distribution):

$$(w_v)_{v \in V} \stackrel{d}{=} (W_v)_{v \in V}.$$

However, the original VBT algorithm just snaps the query time r to the nearest element of V , so its output distribution is imprecise at all points $r \in [t_0, t_1] \setminus V$. We can fix this by using an interpolation based on the distribution of the Brownian bridge:

$$\begin{aligned} \text{for } s < r < u \quad (W_r | W_s, W_u) &\sim \mathcal{N}\left(W_s + \frac{r-s}{u-s}W_{s,u}, \frac{(r-s)(u-r)}{u-s}\right), \text{ so we set} \\ \text{final_interpolation}(s, r, u, w_s, w_u, \rho) &= w_s + \frac{r-s}{u-s}(w_u - w_s) + \sqrt{\frac{(r-s)(u-r)}{u-s}} \mathcal{N}(0, \mathbf{I}_d, \rho) \end{aligned} \quad (2)$$

The following proposition states that our generated path now exactly matches the desired distribution, as long as we draw at most one sample between each two consecutive points in V .

Theorem 3.1 (Distributional correctness of VBT). *Let ρ be a PRNG seed, let $t_0 < t_1 \in \mathbb{R}$, $L, d \in \mathbb{N}$, $\varepsilon = (t_1 - t_0)2^{-L}$ and*

$$w_r := \text{VirtualBrownianTree.eval}(r, [t_0, t_1], \rho, d, \varepsilon),$$

where the *VirtualBrownianTree* is implemented using the *final_interpolation* from Eq. (2).

Let $V = \{t_0 + (t_1 - t_0)k2^{-L} : k \in \{0, 1, \dots, 2^L\}\}$ be the set of vertices of the VBT and let $S = \{r_1, \dots, r_N\} \subset [t_0, t_1]$ be a set of query times such that for all $0 \leq n < N$ we have $r_n \leq r_{n+1}$ and $|V \cap [r_n, r_{n+1}]| \geq 1$.

If W is a Brownian motion and ρ was chosen uniformly at random (but is fixed throughout), then the joint distribution of w sampled at points from S matches the joint distribution of W sampled at the same points:

$$(w_r)_{r \in S} \stackrel{d}{=} (W_r)_{r \in S}.$$

Proof. This is a special case of Theorem 4.2, in which we extend this result to include Lévy areas as well. \square

3.2 Chen’s relation for Lévy area

Recall the space-time Lévy area H and the space-time-time Lévy area K from Definition 2.2.

In order for the *VirtualBrownianTree* to generate these Lévy areas, we must devise versions of the *bridge* and *final_interpolation* functions that work not only for the Brownian motion W , but for the pair (W, H) or the triple (W, H, K) . The first step is finding a way of concatenating Lévy areas over consecutive intervals.

For times $0 \leq s \leq t \leq u$, Brownian motion can be concatenated via addition $W_{s,u} = W_{s,t} + W_{t,u}$, while concatenating Lévy areas requires a special case of Chen’s relation [Che57], which uses rescaled Lévy areas.

Definition 3.2 (Rescaled Lévy areas). Let $0 \leq s < t$ be two times. Then the rescaled space-time Lévy area \bar{H} and space-time-time Lévy area \bar{K} are given by

$$\bar{H}_{s,t} = (t-s)H_{s,t}, \quad \bar{K}_{s,t} = (t-s)^2 K_{s,t}.$$

Theorem 3.3 (Chen's relation). For times $0 \leq s < t < u$, Chen's relation is given by

$$\begin{aligned} W_{s,u} &= W_{s,t} + W_{t,u}, \\ \bar{H}_{s,u} &= \bar{H}_{s,t} + \bar{H}_{t,u} + \frac{u-s}{2} B_t^{s,u}, \\ \bar{K}_{s,u} &= \bar{K}_{s,t} + \bar{K}_{t,u} + \frac{u-t}{2} \bar{H}_{s,t} - \frac{t-s}{2} \bar{H}_{t,u} + \frac{(u-t)^2 - (t-s)^2}{12} B_t^{s,u}. \end{aligned} \tag{3}$$

where $B_t^{s,u} := W_{s,t} - \frac{t-s}{u-s} W_{s,u}$ denotes the Brownian bridge associated with W on $[s, u]$.

The proof of this theorem and a visualisation of Chen's relation for space-time Lévy area are in Appendix B.1.

3.2.1 Lévy area as a singly-indexed process

Note that unlike the Brownian motion, which has a value W_t at any time t , the Lévy areas are only defined for time intervals, i.e. we give a meaning to $H_{s,t}$, but not to H_t . Dealing with such a doubly indexed process in numerical applications can be difficult. In particular, when computing $H_{s,t}$, rather than just running Algorithm 1 for s and t separately and then taking the difference, an entirely different approach would have to be devised. Fortunately, we can use Chen's relation to tackle this.

By setting $s = 0$ in Eq. (3), we obtain

$$\begin{aligned} \bar{H}_{t,u} &= \bar{H}_{0,u} - \bar{H}_{0,t} - \frac{1}{2}(uW_t - tW_u) \\ \bar{K}_{t,u} &= \bar{K}_{0,u} - \bar{K}_{0,t} - \frac{u-t}{2} \bar{H}_{0,t} + \frac{t}{2} \bar{H}_{t,u} - \frac{u-2t}{12} (uW_t - tW_u). \end{aligned} \tag{4}$$

Let $Y_{s,r} := (W_{s,r}, H_{s,r}, K_{s,r})$ for any $0 \leq s \leq r$. Then, by above, knowing any two of $Y_{0,t}, Y_{0,u}, Y_{t,u}$ lets one compute the third. The same holds when Y is instead just (W, H) , or when we use the rescaled version $\bar{Y}_{s,r} = (W_{s,r}, \bar{H}_{s,r}, \bar{K}_{s,r})$. From here on, we will use $Y_{0,r}$ and Y_r interchangeably (likewise for H and K).

3.3 Midpoint Brownian bridge for Lévy area

Let $0 \leq s < u$ and $t = \frac{s+u}{2}$. To incorporate Lévy areas into the **bridge** function we need to find a way to generate the midpoint values \bar{Y}_t given \bar{Y}_s and \bar{Y}_u . This can be done using theorems 6.1.6 and 6.1.8 from [Fos20]. This midpoint bridge formula will differ depending on if we are working with just the process $Y = (W, H)$, or with the full $Y = (W, H, K)$. These formulae will be stated separately.

3.3.1 Space-time Lévy area only

Given $W_s, W_u, \bar{H}_s, \bar{H}_u$, we want to generate W_t and \bar{H}_t . We first compute $W_{s,u}, \bar{H}_{s,u}$ using Eq. (4). The following corollary of Theorem 3.6 [Fos20] gives the distribution at the midpoint:

Corollary 3.4 (Midpoint Brownian bridge for (W, H)). Let $0 \leq s < u$ and $t = \frac{s+u}{2}$. Then

$$\begin{aligned} W_{s,t} &= \frac{1}{2}W_{s,u} + \frac{3}{2}H_{s,u} + Z, & W_{t,u} &= \frac{1}{2}W_{s,u} - \frac{3}{2}H_{s,u} - Z, \\ H_{s,t} &= \frac{1}{4}H_{s,u} - \frac{1}{2}Z + \frac{1}{2}N, & H_{t,u} &= \frac{1}{4}H_{s,u} - \frac{1}{2}Z - \frac{1}{2}N, \end{aligned}$$

where $Z \sim \mathcal{N}(0, \frac{1}{16}(u-s))$, $N \sim \mathcal{N}(0, \frac{1}{12}(u-s))$, $W_{s,u}$ and $\bar{H}_{s,u}$ are all independent.

Proof. Follows directly from Theorem 3.6 by setting $r = t = \frac{s+u}{2}$. \square

Since we are working with the rescaled Lévy area, we can write the above as

$$W_{s,t} = \frac{1}{2}W_{s,u} + \frac{3}{2(u-s)}\bar{H}_{s,u} + Z, \quad \bar{H}_{s,t} = \frac{1}{8}\bar{H}_{s,u} - \frac{u-s}{4}Z + \frac{u-s}{4}N. \quad (5)$$

Finally using Chen's relation again we can compute W_t, \bar{H}_t from $W_s, \bar{H}_s, W_{s,t}$ and $\bar{H}_{s,t}$.

3.3.2 Both space-time and space-time-time Lévy areas

Suppose instead, we are given $(W, \bar{H}, \bar{K})_s, (W, \bar{H}, \bar{K})_u$ and we want to generate $(W, \bar{H}, \bar{K})_t$. We first compute $W_{s,u}, \bar{H}_{s,u}, \bar{K}_{s,u}$ using Eq. (4). The midpoint Brownian bridge is given by Theorem 6.1.8 from [Fos20]:

Theorem 3.5 (Midpoint Brownian bridge for (W, H, K)). *Let t denote the midpoint $t = s + \frac{1}{2}(u-s)$. Then,*

$$\begin{aligned} W_{s,t} &= \frac{1}{2}W_{s,u} + \frac{3}{2}H_{s,u} + Z & W_{t,u} &= \frac{1}{2}W_{s,u} - \frac{3}{2}H_{s,u} - Z, \\ H_{s,t} &= \frac{1}{4}H_{s,u} + \frac{15}{4}K_{s,u} - \frac{1}{2}Z + X_1, & H_{t,u} &= \frac{1}{4}H_{s,u} - \frac{15}{4}K_{s,u} - \frac{1}{2}Z - X_1, \\ K_{s,t} &= \frac{1}{8}K_{s,u} - \frac{1}{2}X_1 + X_2, & K_{t,u} &= \frac{1}{8}K_{s,u} - \frac{1}{2}X_1 - X_2, \end{aligned}$$

where $W_{s,u}, H_{s,u}, K_{s,u}, Z, X_1, X_2$ are independent Gaussian random variables with

$$Z \sim \mathcal{N}\left(0, \frac{u-s}{16}\right), \quad X_1 \sim \mathcal{N}\left(0, \frac{u-s}{768}\right), \quad X_2 \sim \mathcal{N}\left(0, \frac{u-s}{2880}\right).$$

The proof can be found in Appendix B.2.

Expressing this in terms of rescaled Lévy areas, the formula for W is the same as in Eq. (5), and

$$\bar{H}_{s,t} = \frac{1}{8}\bar{H}_{s,u} + \frac{15}{8(u-s)}\bar{K}_{s,u} - \frac{u-s}{4}Z + \frac{u-s}{2}X_1, \quad \bar{K}_{s,t} = \frac{1}{32}\bar{K}_{s,u} - \frac{(u-s)^2}{8}X_1 + \frac{(u-s)^2}{4}X_2.$$

Finally, we can use Chen's relation again to compute $W_t, \bar{H}_t, \bar{K}_t$.

3.4 Interpolation between dyadic points for Lévy area

To derive the Lévy-area-endowed version of the `final_interpolation` function, we need to be able to generate the Brownian motion and Lévy areas at any intermediate time $r \in [s, u]$. The (W, H) case is taken from [Fos20, Theorem 6.1.4], whereas the (W, H, K) case is new here.

3.4.1 Space-time Lévy area

Given $W_s, W_u, \bar{H}_s, \bar{H}_u$, we want to generate W_r and \bar{H}_r . We first compute $W_{s,u}$ and $\bar{H}_{s,u}$ using Chen's relation as in Section 3.3.1, and rescale to obtain $H_{s,u} = \frac{1}{u-s}\bar{H}_{s,u}$.

Theorem 6.1.4 from [Fos20] gives the required update rule.

Theorem 3.6 (General Brownian bridge for (W, H)). *Let $r \in [s, u]$ be some time and let W denote a standard Brownian motion. Then*

$$\begin{aligned} W_{s,r} &= \frac{r-s}{u-s}W_{s,u} + \frac{6(r-s)(u-r)}{(u-s)^2}H_{s,u} + \frac{2(a+b)}{u-s}X_1, \\ H_{s,r} &= \frac{(r-s)^2}{(u-s)^2}H_{s,u} - \frac{a}{r-s}X_1 + \frac{c}{r-s}X_2, \end{aligned}$$

where $W_{s,u}, H_{s,u}, X_1, X_2$ are independent Gaussian random variables with $X_1, X_2 \sim \mathcal{N}(0, 1)$ and

$$\begin{aligned} a &:= \frac{(r-s)^{\frac{7}{2}}(u-r)^{\frac{1}{2}}}{2(u-s)d}, & b &:= \frac{(r-s)^{\frac{1}{2}}(u-r)^{\frac{7}{2}}}{2(u-s)d}, \\ c &:= \frac{\sqrt{3}(r-s)^{\frac{3}{2}}(u-r)^{\frac{3}{2}}}{6d}, & d &:= \sqrt{(r-s)^3 + (u-r)^3}. \end{aligned}$$

Having generated $W_{s,r}$ and $H_{s,r}$ via the theorem above, we use Chen's relation to compute W_r and \bar{H}_r .

3.4.2 Both space-time and space-time-time Lévy areas

We consider $Y := (W, H, K)$, and $\bar{Y} = (W, \bar{H}, \bar{K})$. Then, given \bar{Y}_s and \bar{Y}_u , we want to generate Y_r . We first compute $W_{s,u}, \bar{H}_{s,u}, \bar{K}_{s,u}$ using Chen's relation as in Section 3.3.2, and rescale to obtain $H_{s,u} = \frac{1}{u-s}\bar{H}_{s,u}$ and $K_{s,u} = \frac{1}{(u-s)^2}\bar{K}_{s,u}$. The following theorem (which is new here) gives a rule for generating $Y_{s,r}$ conditional on $Y_{s,u}$, which in this case is equivalent to conditioning on Y_s and Y_u . The proof is in Appendix B.3

Theorem 3.7 (General Brownian bridge for (W, H, K)). *For any $0 \leq s < u$ and $r \in [s, u]$ the distribution of $Y_{s,r}$ conditioned on $Y_{s,u}$ is Gaussian with the following mean:*

$$\begin{aligned} \mathbb{E}[W_{s,r}|Y_{s,u}] &= \frac{r-s}{u-s}W_{s,u} + 6\frac{(r-s)(u-r)}{(u-s)^2}H_{s,u} + 120\frac{(r-s)(u-r)(\frac{1}{2}(u+s)-r)}{(u-s)^3}K_{s,u}, \\ \mathbb{E}[H_{s,r}|Y_{s,u}] &= \frac{(r-s)^2}{(u-s)^2}H_{s,u} + 30\frac{(r-s)^2(u-r)}{(u-s)^3}K_{s,u}, \\ \mathbb{E}[K_{s,r}|Y_{s,u}] &= \frac{(r-s)^3}{(u-s)^3}K_{s,u}, \end{aligned} \tag{6}$$

and the following covariance matrix:

$$\Sigma_r := \mathbb{E}\left[(Y_{s,r} - \mathbb{E}[Y_{s,r}|Y_{s,u}])(Y_{s,r} - \mathbb{E}[Y_{s,r}|Y_{s,u}])^T \mid Y_{s,u}\right] = \begin{bmatrix} \Sigma_r^{WW} & \Sigma_r^{WH} & \Sigma_r^{WK} \\ \Sigma_r^{WH} & \Sigma_r^{HH} & \Sigma_r^{HK} \\ \Sigma_r^{WK} & \Sigma_r^{HK} & \Sigma_r^{KK} \end{bmatrix}, \tag{7}$$

with coefficients

$$\begin{aligned} \Sigma_r^{WW} &= \frac{(r-s)(u-r)\left((2r-u-s)^4 + 4(r-s)^2(u-r)^2\right)}{(u-s)^5}, \\ \Sigma_r^{WH} &= -\frac{(r-s)^3(u-r)\left((r-s)^2 - 3(r-s)(u-r) + 6(u-r)^2\right)}{2(u-s)^5}, \\ \Sigma_r^{WK} &= \frac{(r-s)^4(u-r)(2r-u-s)}{12(u-s)^5}, \\ \Sigma_r^{HH} &= \frac{r-s}{12}\left(1 - \frac{(r-s)^3\left((r-s)^2 + 2(r-s)(u-r) + 16(u-r)^2\right)}{(u-s)^5}\right), \\ \Sigma_r^{HK} &= -\frac{(r-s)^5(u-r)}{24(u-s)^5}, \quad \Sigma_r^{KK} = \frac{r-s}{720}\left(1 - \frac{(r-s)^5}{(u-s)^5}\right). \end{aligned}$$

Remark 3.8. $\mathbb{E}[W_{s,r}|Y_{s,u}]$ follows a cubic polynomial, which was first shown in [FLO20] and [Hab21].

We can generate the multivariate normal $\widehat{Y}_{s,r} \sim \mathcal{N}(0, \widehat{\Sigma}_r)$ using a singular-value decomposition, which is not very computationally expensive, since $\widehat{\Sigma}_r$ is only a 3×3 matrix. A slightly more efficient choice would be the Cholesky decomposition, but $\widehat{\Sigma}_r$ is singular when $r = s$ or $r = u$, so the Cholesky decomposition can become inaccurate when $|r - s|$ or $|u - r|$ are small.

Finally we compute $(W_{s,r}, H_{s,r}, K_{s,r}) = \widehat{Y}_{s,r} + \mathbb{E}[Y_{s,r}|Y_{s,u}]$, rescale the Lévy areas and use Chen’s relation to compute W_r, H_r and K_r .

4 Implementation

We can now incorporate the Lévy-area-endowed versions of the `bridge` and `final_interpolation` functions from Sections 3.3 and 3.4 respectively into the `VirtualBrownianTree` algorithm. The full pseudocode for `bridge` and `final_interpolation` can be found in Appendix A.

In the interest of efficiency and numerical stability we also introduce two further changes to the algorithm:

- Instead of Y_s and Y_u , we keep track of $\overline{Y}_s, \overline{Y}_u$ and $\overline{Y}_{s,u}$ ¹ which lets us avoid repeatedly rescaling the Lévy areas and saves us an additional application of Chen’s relation in the `bridge` function.
- We internally normalise the interval of definition (see Section 4.1).

4.1 Interval Normalisation

In order to make the calculations simpler, as well as more efficient and numerically stable, we modify the `VirtualBrownianTree` so that its interval of definition $[t_0, t_1]$ is internally normalised to $[0, 1]$. The tolerance for discretising the interval is also rescaled accordingly. When the Brownian motion and Lévy areas are evaluated at a given time r , this is first rescaled to $\hat{r} := \frac{r-t_0}{t_1-t_0}$. After the computations are done in the normalized space, the results are then rescaled back from $[0, 1]$ to the original interval $[t_0, t_1]$ using Brownian scaling, i.e. $X_r^{\text{out}} = \sqrt{t_1 - t_0} X_{\hat{r}}$ for $X \in \{W, H, K\}$.

This provides three main benefits:

- With normalisation, all the times appearing in the tree are exact dyadic rationals, and are thus represented exactly in floating-point format. This eliminates many potential sources of error.
- The midpoint update rule has a nicer form and is about 20% faster to compute.
- If t_1 and t_0 are very large, but close together, the original implementation could suffer from catastrophic cancellation errors. Without normalisation, these would appear in many calculations as we descend the tree, causing significant compounding errors. These are avoided with our construction.

4.2 The main loop

Our algorithm depends on a `levy_area` parameter, governing which types of Lévy area will be computed. We present the case when `levy_area = 'space-time-time'`, i.e. when all of W, H and K are being computed. The (W, H) case with `levy_area = 'space-time'` is obtained by simply removing all references to K , or removing both H and K when `levy_area = 'none'`, so only Brownian increments are generated.

We introduce a helper function `rescale` which converts $\overline{Y} = (W, \overline{H}, \overline{K})$ to $Y = (W, H, K)$.

¹Note that this is just for computational convenience inside a single evaluation of the VBT, and should not be confused with computing Y_{r_0, r_1} . In that case we first separately evaluate the VBT for Y_{r_0} and Y_{r_1} , before computing Y_{r_0, r_1} from these.

Algorithm 2 rescale

Input: h - time increment, \bar{Y} - Brownian motion and Lévy areas
 $(W, \bar{H}, \bar{K}) \leftarrow \bar{Y}$
 $H \leftarrow h^{-1}\bar{H}, K \leftarrow h^{-2}\bar{K}$
return (W, H, K)

Now we can state the algorithm for evaluating the `VirtualBrownianTree` at a single time r .

Algorithm 3 `VirtualBrownianTree.eval` with space-time-time Lévy area

Input: r - evaluation time, $[t_0, t_1]$ - interval of definition, ρ - PRNG seed, d - dimension, ε - tolerance.

Result: Approximation to $(W_{t_0, r}, H_{t_0, r}, K_{t_0, r})$

```
 $\hat{r} \leftarrow \frac{r-t_0}{t_1-t_0}$   
 $l \leftarrow 0, s \leftarrow 0, u \leftarrow 1$  ▷  $l$  is the current level in the tree and  $u - s = 2^{-l}$ .  
 $\rho, \hat{\rho}_W, \hat{\rho}_H, \hat{\rho}_K \leftarrow \text{split\_seed}(\rho, 4)$   
 $W_u \leftarrow \mathcal{N}(0, \mathbf{I}_d, \hat{\rho}_W), H_u \leftarrow \mathcal{N}(0, \frac{1}{12}\mathbf{I}_d, \hat{\rho}_H), K_u \leftarrow \mathcal{N}(0, \frac{1}{720}\mathbf{I}_d, \hat{\rho}_K)$   
 $\bar{Y}_s \leftarrow (0, 0, 0), \bar{Y}_u \leftarrow (W_u, H_u, K_u), \bar{Y}_{s,u} \leftarrow \bar{Y}_u$   
while  $2^l > \frac{\varepsilon}{t_1-t_0}$  do  
   $\rho_1, \rho_2, \hat{\rho} \leftarrow \text{split\_seed}(\rho, 3)$   
   $t \leftarrow s + 2^{l+1}$   
   $\bar{Y}_t, \bar{Y}_{s,t}, \bar{Y}_{t,u} \leftarrow \text{bridge}(l, s, \bar{Y}_s, \bar{Y}_u, \bar{Y}_{s,u}, \hat{\rho})$   
  if  $\hat{r} \leq t$  then ▷ Descend into the left child.  
     $\rho \leftarrow \rho_1$   
     $s \leftarrow s, u \leftarrow t$   
     $\bar{Y}_s \leftarrow \bar{Y}_s, \bar{Y}_u \leftarrow \bar{Y}_t, \bar{Y}_{s,u} \leftarrow \bar{Y}_{s,t}$   
  else ▷ Descend into the right child.  
     $\rho \leftarrow \rho_2$   
     $s \leftarrow t, u \leftarrow u$   
     $\bar{Y}_s \leftarrow \bar{Y}_t, \bar{Y}_u \leftarrow \bar{Y}_u, \bar{Y}_{s,u} \leftarrow \bar{Y}_{t,u}$   
  end if  
   $l \leftarrow l + 1$   
end while  
 $\bar{Y}_{\hat{r}} \leftarrow \text{final\_interpolation}(s, r, u, \bar{Y}_s, \bar{Y}_u, \bar{Y}_{s,u}, \rho)$   
 $Y_{\hat{r}} \leftarrow \text{rescale}(\hat{r}, \bar{Y})$   
return  $\sqrt{t_1 - t_0} Y_{\hat{r}}$  ▷ Undo the effects of interval normalisation.
```

The usual use case is when instead of a single evaluation time r , we are provided with an interval $[r_0, r_1] \subseteq [t_0, t_1]$ and want the value of Y_{r_0, r_1} . In this case, we first compute $\bar{Y}_{\hat{r}_0}$ and $\bar{Y}_{\hat{r}_1}$ using Algorithm 3 (stopping at the line with `final_interpolation`) and apply Chen's relation (Eq. (3)) to obtain $\bar{Y}_{\hat{r}_0, \hat{r}_1}$. We then compute $Y_{\hat{r}_0, \hat{r}_1} = \text{rescale}(\hat{r}_1 - \hat{r}_0, \bar{Y}_{\hat{r}_0, \hat{r}_1})$ and finally undo the normalisation: $Y_{r_0, r_1} = \sqrt{t_1 - t_0} Y_{\hat{r}_0, \hat{r}_1}$.

4.3 Matching the true distribution

Due to our careful construction of the `final_interpolation` function, we can now prove the general case of Theorem 3.1, which also holds when Lévy area is present. We have already proven in Section 3.4 that conditional on Y_s and Y_u , the output of `final_interpolation`($l, s, \bar{Y}_s, \bar{Y}_u, \bar{Y}_{s,u}, \rho$) has the correct distribution. Theorems 3.4 and 3.5 further show that for all points in $V = \{t_0 + (t_1 - t_0)k2^{-L} : k \in \{0, 1, \dots, 2^L\}\}$ the generated random variables $(Y_v)_{v \in V}$ have the correct joint distribution.

We first need the following lemma:

Lemma 4.1 (Y is a Markov process). *The processes $(W_t, H_t, K_t)_{t \geq 0}$, $(W_t, \bar{H}_t, \bar{K}_t)_{t \geq 0}$, $(W_t, H_t)_{t \geq 0}$, and $(W_t, \bar{H}_t)_{t \geq 0}$ are all Markov processes.*

Proof. Rearranging the definitions of \bar{H} and \bar{K} we obtain

$$\begin{aligned}\bar{H}_t &= \int_0^t W_s ds - \frac{t}{2}W_t, \\ \bar{K}_t &= \frac{t}{2} \int_0^t W_s ds - \int_0^t sW_s ds - W_t \int_0^t \frac{s}{t} \left(\frac{t}{2} - s \right) ds.\end{aligned}$$

Using this, we can write the process (W_t, H_t, K_t) as an SDE:

$$\begin{aligned}dW_t &= dW_t, & d\bar{H}_t &= \frac{W_t}{2} dt - \frac{r}{2} dW_t, \\ d\bar{K}_t &= \left(\bar{H}_t - \frac{7}{12}tW_t \right) dt + \frac{t^2}{12} dW_t.\end{aligned}\tag{8}$$

Since all of the SDE coefficients only depend on the current state of (W_t, H_t, K_t) , the process is Markovian.

Moreover, as (W_r, H_r, K_r) is a deterministic function of $(W_r, \bar{H}_r, \bar{K}_r)$, it is also Markovian. The same arguments apply for the pair (W, H) . \square

We are now ready to prove the general version of Theorem 3.1.

Theorem 4.2 (Distributional correctness of the Virtual Brownian Tree with Lévy area). *Let Y be any of W , (W, H) , or (W, H, K) and let `levy_area` be set to ‘none’, ‘space-time’, or ‘space-time-time’ respectively. Let $0 \leq t_0 < t_1$, $L, d \in \mathbb{N}$, $\varepsilon = (t_1 - t_0)2^{-L}$ and let ρ be a PRNG seed. Define the generated path y as*

$$y_r := \text{VirtualBrownianTree.eval}(r, [t_0, t_1], \rho, d, \varepsilon, \text{levy_area}).$$

Let $V = \{t_0 + (t_1 - t_0)k2^{-L} : k \in \{0, 1, \dots, 2^L\}\}$ be the set of vertices of the VBT and let $S = \{r_1, \dots, r_N\} \subset [t_0, t_1]$ be a set of query-times such that for all $0 \leq n < N$ we have $r_n \leq r_{n+1}$ and $|V \cap [r_n, r_{n+1}]| \geq 1$.

Suppose that the seed ρ is chosen uniformly at random (but is fixed throughout). Then the joint distribution of y sampled at points from S matches the joint distribution of Y sampled at the same points. That is,

$$(y_r)_{r \in S} \stackrel{d}{=} (Y_r)_{r \in S}.$$

Proof. By the monotone class theorem, it is enough to prove that for any choice of measurable sets $G_1, \dots, G_N \subseteq \mathbb{R}^d$ we have $\mathbb{P}(y_{r_n} \in G_n \text{ for } n = 1, \dots, N) = \mathbb{P}(Y_{r_n} \in G_n \text{ for } n = 1, \dots, N)$ or equivalently

$$\mathbb{E} \left[\prod_{n=1}^N \mathbb{1}_{G_n}(y_{r_n}) \right] = \mathbb{E} \left[\prod_{n=1}^N \mathbb{1}_{G_n}(Y_{r_n}) \right].$$

For $r \in [t_0, t_1]$, we write $\lceil r \rceil_V := \min\{v \in V : v \geq r\}$ and $\lfloor r \rfloor_V := \max\{v \in V : v \leq r\}$ (note that these are always well defined since $t_0, t_1 \in V$).

We will make use of the following facts:

1. Due to our PRNG-splitting method, the keys at the leaves of the `VirtualBrownianTree` are independent and hence if $t_0 \leq q < r \leq t_1$ and $V \cap [q, r]$ is non-empty, then y_r and y_q are conditionally independent given $y_{\lfloor q \rfloor_V}, y_{\lceil q \rceil_V}, y_{\lfloor r \rfloor_V}, y_{\lceil r \rceil_V}$.
2. If $r \in [t_0, t_1]$ and $s = \lfloor r \rfloor_V, u = \lceil r \rceil_V$ then by our choice of interpolation (see theorems 3.6 and 3.7)

$$(y_r | y_s, y_u) \stackrel{d}{=} (Y_r | Y_s = y_s, Y_u = y_u).$$

3. By theorems 3.4 and 3.5, we have $(y_v)_{v \in V} \stackrel{d}{=} (Y_v)_{v \in V}$.
4. By Lemma 4.1, Y is Markovian, so for any $t \geq 0$, the processes $(Y_s)_{s \leq t}$ and $(Y_{t,s})_{s \geq t}$ are independent conditional on Y_t . This implies that Y has the same property as was shown for y in fact 1 above.

Using the above properties, we have

$$\begin{aligned} \mathbb{E} \left[\prod_{n=1}^N \mathbb{1}_{G_n}(y_{r_n}) \right] &= \mathbb{E} \left[\mathbb{E} \left[\prod_{n=1}^N \mathbb{1}_{G_n}(y_{r_n}) \mid (y_v)_{v \in V} \right] \right] && \text{(tower law)} \\ &= \mathbb{E} \left[\prod_{n=1}^N \mathbb{E} \left[\mathbb{1}_{G_n}(y_{r_n}) \mid y_{\lfloor r_n \rfloor_V}, y_{\lceil r_n \rceil_V} \right] \right] && \text{(fact 1)} \\ &= \mathbb{E} \left[\prod_{n=1}^N \mathbb{E} \left[\mathbb{1}_{G_n}(Y_{r_n}) \mid Y_{\lfloor r_n \rfloor_V} = y_{\lfloor r_n \rfloor_V}, Y_{\lceil r_n \rceil_V} = y_{\lceil r_n \rceil_V} \right] \right] && \text{(fact 2)} \\ &= \mathbb{E} \left[\prod_{n=1}^N \mathbb{E} \left[\mathbb{1}_{G_n}(Y_{r_n}) \mid Y_{\lfloor r_n \rfloor_V}, Y_{\lceil r_n \rceil_V} \right] \right] && \text{(fact 3)} \\ &= \mathbb{E} \left[\mathbb{E} \left[\prod_{n=1}^N \mathbb{1}_{G_n}(Y_{r_n}) \mid (Y_v)_{v \in V} \right] \right] = \mathbb{E} \left[\prod_{n=1}^N \mathbb{1}_{G_n}(Y_{r_n}) \right] && \text{(fact 4 \& tower law)} \end{aligned}$$

□

Remark 4.3. The key assumption here is that there is at most one sample point between each two consecutive dyadic points $v, v' \in V$, i.e. $|S \cap [v, v']| \leq 1$. Without this requirement, we can find a simple counterexample. Let $q, r \in (v, v')$ and for simplicity consider the case $Y = W$. When evaluating w_r and w_q , the same key is used in the call to `final_interpolation`, and hence the Z in the computation of w_r is the same as that in w_q . Therefore, knowing $w_v, w_{v'}$ and w_r lets us deterministically compute the value of w_q . However, W_q is not deterministic after we fix $W_v, W_{v'}$ and W_r . Therefore, the joint distribution of (w_r, w_q) cannot be the same as that of (W_r, W_q) .

5 Application to adaptive SDE solvers

To conclude, we will demonstrate how the combination of adaptive time-stepping and high order solvers (which rely on Lévy areas) can result in significant speed-ups for SDE simulation.

VBT time complexity. The Virtual Brownian Tree is based on binary search, so a single evaluation takes $\mathcal{O}(\log(\frac{1}{\varepsilon}))$ time, where ε is the user-specified tolerance. If we are using an adaptive solver with a minimal step size of h_{\min} , Theorem 4.2 tells us that as long as $\varepsilon \leq h_{\min}$, then all Brownian samples drawn by the solver will have exactly the correct joint distribution. Therefore, if the solver takes n computational steps, the total time complexity of a solve will be $\mathcal{O}(-\log(h_{\min})n)$.

5.1 Cox-Ingersoll-Ross model

Consider the Cox-Ingersoll-Ross (CIR) model from mathematical finance, in Stratonovich form:

$$dX_t = a(\tilde{b} - X_t)dt + \sigma\sqrt{X_t} \circ dW_t, \quad \tilde{b} := b - \frac{\sigma^2}{4a} \quad (9)$$

where $a, b, \sigma > 0$ are the mean reversion speed, mean reversion level, and volatility parameters respectively, and W is a 1-dimensional Brownian motion. It was proven by [HJ19] that for any constant step size solver, its SOC (recall Definition 2.1) can be made arbitrarily small by increasing the volatility σ .

The convergence of adaptive solvers is still an open question. In [GL97] and [Fos23] the authors prove that adaptive solvers converge to the correct limit given some assumptions about the SDEs or the step-size controller, but [Fos23] also present a counterexample when these assumptions are violated. Unfortunately, these theorems do not apply to the CIR model due to a non-Lipschitz diffusion coefficient – so we will empirically check the correctness of convergence.

In our experiment, we compare two solvers: the Drift-Implicit Euler (DIE) solver by [Alf05] and a High-order Strang splitting (HoSts) solver by [FRS24], both with constant and adaptive time-stepping. In addition to being high-order, the HoSts solver can ensure that its solution is always positive as long as $\tilde{b} \geq 0$.

To design our step-size controller, we use the mean square error propagation principle [Fos23], which asserts that unlike ODEs, where all L_p errors propagate linearly, in SDEs it is the mean square errors that propagate linearly. Hence, to control the global error, we bound the local errors by $\epsilon_{\text{local}}^2 \leq Ch\varepsilon^2$ where h is the length of the current step, ε is the global error tolerance and C is a proportionality constant. While ϵ_{local} can be estimated using embedded methods [Fos23], or half-stepping,² we use an analytic estimate specific to CIR [Fos20]: $\epsilon_{\text{local}} \propto \left| \frac{ab\sigma^2}{2X_t} \right| h^2$. This gives rise to a simple step-size controller, which sets $h \approx (X_t \varepsilon)^{\frac{2}{3}}$. The code for our numerical experiments is available at github.com/andyElking/Single-seed_BrownianMotion.

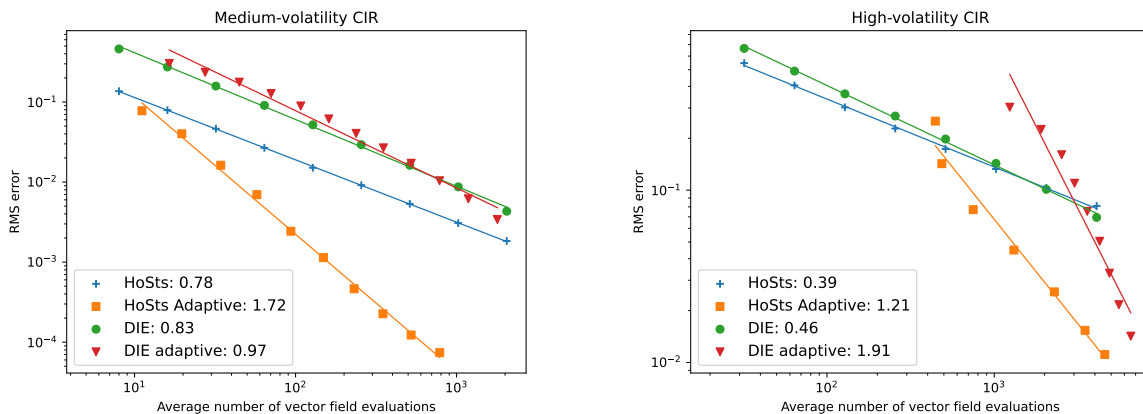


Figure 3: Comparison of the HoSts solver and Drift-Implicit Euler applied to the CIR process both with constant step size and adaptive time-stepping. We use $a = b = 1$ with $\sigma = 1.5$ (left) and $\sigma = 2.5$ (right). The SOC of each solver is written in the legend. The results are averaged over 1000 random seeds.

²Half stepping means that in each step, the solver makes a coarse computation over the whole step, as well as a finer computation with two half-steps, and takes the difference of the results as the local error.

5.2 Third order Langevin solver

To demonstrate the combined capabilities of space-time-time Lévy area and adaptive time-stepping, we turn to a Markov Chain Monte Carlo (MCMC) algorithm based on the underdamped (or kinetic) Langevin diffusion (ULD). Using ULD for MCMC has recently received significant attention [Che+18b; RV23; DR20; SZ21], as it is the stochastic equivalent of Hamiltonian Monte Carlo (HMC) [CFG14]. ULD is given by:

$$\begin{aligned} d\mathbf{x}_t &= \mathbf{v}_t dt \\ d\mathbf{v}_t &= -\gamma \mathbf{v}_t dt - u \nabla f(\mathbf{x}_t) dt + \sqrt{2\gamma u} dW_t, \end{aligned} \tag{10}$$

where $\mathbf{x}_t, \mathbf{v}_t \in \mathbb{R}^d$, W is a d -dimensional BM, $\gamma, u \in \mathbb{R}$ are the friction and damping coefficients and $f : \mathbb{R}^d \rightarrow \mathbb{R}$ is a potential function. The stationary density of this SDE is $p(x) = C \exp(-f(x))$ where C is a normalising constant.

ULD is a rare type of SDE for which a third order solver has been found – namely the Shifted-ODE Runge-Kutta Three (SORT) solver by [FLO21], which requires space-time-time Lévy area as input. and can be used adaptively via half-stepping. We compare SORT to the Euler-Maruyama method, which is the usual discretisation used for Langevin Monte Carlo, as well as to SRA1 – a method developed for additive-noise SDEs by [Röß10]. We also compare to the No U-Turn Sampler as the standard choice for MCMC. For adaptive stepping we use a PI controller with $K_P = 0.1$ and $K_I = 0.3$ which are the recommended values for SDEs by [IJE15]. We set the relative tolerance to 0 and vary the absolute tolerance to obtain the graph on the right of Fig. 4.

As the target distribution we chose a common MCMC benchmark called Neal’s funnel [Nea03], given by the pair $x \sim \mathcal{N}(0, 9)$, $y \sim \mathcal{N}(0, \exp(x)\mathbf{I}_9)$. This is particularly challenging for Markov chain algorithms due to the very narrow funnel, which is hard for some samplers to enter into.

SORT with constant steps seems to perform best in the strong convergence graph in Fig. 4, partly because the adaptive version uses half-stepping, which requires 3-times more vector field evaluations per step. However, constant stepping suffers from instabilities which produce points far outside the funnel. Despite removing all outliers with $\|z\| > 100$, constant-step solvers underperformed in Table 1. Furthermore, with adaptive stepping the solver automatically tries to use the minimal number of steps needed to achieve the user-specified precision. Hence, adaptive SORT uses the fewest ∇f evaluations in Table 1.

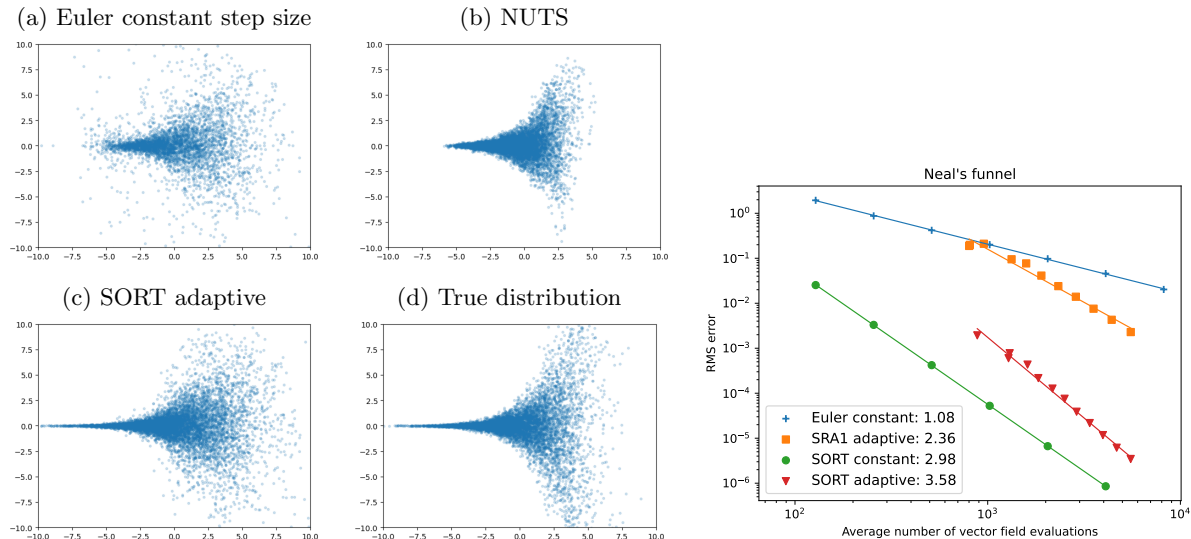


Figure 4: Left: qualitative comparison of Neal’s funnel distributions generated by different methods. Right: The SOC of different solvers on the Neal’s funnel Langevin SDE.

Table 1: A quantitative comparison of NUTS, and ULD MCMC (with constant or adaptive time-stepping) for sampling from Neal’s funnel. The samples were generated using 64 chains of 128 samples, with $\Delta t = 2$ between samples and 16 burn-in iterations. We rescaled the samples by $x' = x/3$, $y' = ye^{-x/2}$, which should result in a 10-dim standard Gaussian. We computed the absolute errors in the mean and the covariance matrix – we report the maximum and average of the entries. For each marginal we performed the Kolmogorov-Smirnov (KS) test and computed the effective sample size (ESS). Results were averaged over 5 random seeds.

Method	∇f evals per sample	Mean error		Cov error		Avg KS P-values	ESS	
		Max	Avg	Max	Avg		Min	Avg
NUTS	700.2	0.79	0.44	0.56	0.16	0.044	0.009	0.021
ULD Euler const	137.0	0.12	0.069	150	4.9	0.0	0.12	0.19
ULD SORT const	274.0	0.20	0.034	42	1.7	0.0	0.12	0.17
ULD SORT adap	59.9	0.20	0.047	0.34	0.029	0.17	0.12	0.13

6 Discussion and open directions

The Langevin Monte Carlo algorithm based on the third order solver SORT in Section 5.2 yielded surprisingly good results using very few gradient evaluations. Nevertheless, since this application is several levels “up the stack” from the primary topic of this paper, we did not pursue it further here. However, a more detailed exploration of this new MCMC algorithm could be of interest, including parameter tuning, dimensional scaling, and experiments on other target distributions, especially ones arising from real data.

While the SORT algorithm is probably not Metropolis adjustable, there is potential to combine other MCMC approaches with adaptive stepping. MALT by [RV23] is one such example. Since VBT always generates the same path given a fixed seed, it could be used to bring adaptive stepping to Multilevel Monte Carlo [Gil08].

MCMC methods normally rely on having very long chains, since they exactly match the target (stationary) distribution only at $t = \infty$. Getting a good estimate on how close the chain is to stationarity is important for determining the burn-in period. Chain couplings were used by [BJV19] for estimating convergence and by [JOA19] to achieve stationarity at a finite time. [Cha+23] extends this to underdamped/kinetic Langevin Monte Carlo by using coupled SDE trajectories which start at different points and use different (constant) step sizes, but are driven by the same noise. Adding adaptive stepping to this construction is a promising application for the Virtual Brownian Tree, since it can guarantee the same Brownian path is provided to both chains, even if the solver uses different step sizes on each of them.

Acknowledgements

AJ thanks the UK National Cyber Security Centre for funding his research and Extropic.ai for funding his work on implementing the Virtual Brownian Tree and high order SDE solvers in DiffraX. AJ and JF would also like to acknowledge support from the Maths4DL programme under EPSRC grant EP/V026259/1 and the Alan Turing Institute. JF and PK were previously supported by the EPSRC Programme Grant “DataSig” EP/S026347/1.

References

- [Alf05] A. Alfonsi. “On the discretization schemes for the CIR (and Bessel squared) processes”. In: *Monte Carlo Methods Appl.* 2005. URL: <https://api.semanticscholar.org/CorpusID:15154545>.
- [BHB04] P. Burrage, R. Herdiana, and K. Burrage. “Adaptive stepsize based on control theory for stochastic differential equations”. In: *Journal of Computational and Applied Mathematics* 170.2 (2004), pp. 317–336. ISSN: 0377-0427. DOI: <https://doi.org/10.1016/j.cam.2004.01.027>. URL: <https://www.sciencedirect.com/science/article/pii/S0377042704000731>.
- [BJV19] N. Biswas, P. E. Jacob, and P. Vanetti. “Estimating Convergence of Markov chains with L-Lag Couplings”. In: *Advances in Neural Information Processing Systems*. Ed. by H. Wallach et al. Vol. 32. Curran Associates, Inc., 2019. URL: https://proceedings.neurips.cc/paper_files/paper/2019/file/aec851e565646f6835e915293381e20a-Paper.pdf.
- [Bro+11] S. Brooks et al. *Handbook of Markov Chain Monte Carlo*. ISSN: CRC Press, 2011. ISBN: 9781420079425. URL: <https://books.google.co.uk/books?id=qfRsAIKZ4rIC>.
- [CC80] J. M. C. Clark and R. J. Cameron. “The maximum rate of convergence of discrete approximations for stochastic differential equations”. In: *Stochastic Differential Systems Filtering and Control*. Springer Berlin Heidelberg, 1980, pp. 162–171.
- [CFG14] T. Chen, E. B. Fox, and C. Guestrin. *Stochastic Gradient Hamiltonian Monte Carlo*. 2014. arXiv: 1402.4102 [stat.ME].
- [Cha+23] N. K. Chada et al. *Unbiased Kinetic Langevin Monte Carlo with Inexact Gradients*. 2023. arXiv: 2311.05025 [stat.CO].
- [Che+18a] R. T. Q. Chen et al. “Neural Ordinary Differential Equations”. In: *Advances in Neural Information Processing Systems*. Ed. by S. Bengio et al. Vol. 31. Curran Associates, Inc., 2018. URL: https://proceedings.neurips.cc/paper_files/paper/2018/file/69386f6bb1dfed68692a24c8686939b9-Paper.pdf.
- [Che+18b] X. Cheng et al. “Underdamped Langevin MCMC: A non-asymptotic analysis”. In: *Proceedings of the 31st Conference On Learning Theory*. Ed. by S. Bubeck, V. Perchet, and P. Rigollet. Vol. 75. Proceedings of Machine Learning Research. PMLR, July 2018, pp. 300–323. URL: <https://proceedings.mlr.press/v75/cheng18a.html>.
- [Che57] K.-T. Chen. “Integration of Paths, Geometric Invariants and a Generalized Baker-Hausdorff Formula”. In: *Annals of Mathematics* 65 (1957), p. 163. URL: <https://api.semanticscholar.org/CorpusID:124765064>.
- [CP13] K. Claessen and M. Pałka. “Splittable pseudorandom number generators using cryptographic hashing”. In: *ACM SIGPLAN Notices* 48 (2013), pp. 47–58.
- [Dav14] A. Davie. “KMT Theory Applied to Approximations of SDE”. In: *Stochastic Analysis and Applications 2014*. Springer International Publishing, 2014, pp. 185–201.
- [Dic07] A. S. Dickinson. “Optimal Approximation of the Second Iterated Integral of Brownian Motion”. In: *Stochastic Analysis and Applications* 25.5 (2007), pp. 1109–1128.
- [DP80] J. Dormand and P. Prince. “A family of embedded Runge-Kutta formulae”. In: *Journal of Computational and Applied Mathematics* 6.1 (1980), pp. 19–26. ISSN: 0377-0427. DOI: [https://doi.org/10.1016/0771-050X\(80\)90013-3](https://doi.org/10.1016/0771-050X(80)90013-3). URL: <https://www.sciencedirect.com/science/article/pii/0771050X80900133>.
- [DR20] A. S. Dalalyan and L. Riou-Durand. “On sampling from a log-concave density using kinetic Langevin diffusions”. In: *Bernoulli* 26.3 (2020), pp. 1956–1988. URL: <https://projecteuclid.org/euclid.bj/1587974530>.
- [FH22] J. Foster and K. Habermann. “Brownian bridge expansions for Lévy area approximations and particular values of the Riemann zeta function”. In: *Combinatorics, Probability and Computing* (2022), pp. 1–28.
- [FLO20] J. Foster, T. Lyons, and H. Oberhauser. “An Optimal Polynomial Approximation of Brownian Motion”. In: *SIAM Journal on Numerical Analysis* 58.3 (2020), pp. 1393–1421. DOI: 10.1137/19M1261912.

- [FLO21] J. Foster, T. Lyons, and H. Oberhauser. *The shifted ODE method for underdamped Langevin MCMC*. 2021. arXiv: 2101.03446 [math.NA].
- [Fos20] J. M. Foster. “Numerical approximations for stochastic differential equations”. PhD thesis. University of Oxford, 2020.
- [Fos23] J. Foster. *On the convergence of adaptive approximations for stochastic differential equations*. 2023. arXiv: 2311.14201 [math.NA].
- [FRS23] J. Foster, G. dos Reis, and C. Strange. *High order splitting methods for SDEs satisfying a commutativity condition*. 2023. arXiv: 2210.17543 [math.NA].
- [FRS24] J. M. Foster, G. dos Reis, and C. Strange. “High Order Splitting Methods for SDEs Satisfying a Commutativity Condition”. In: *SIAM Journal on Numerical Analysis* 62.1 (2024), pp. 500–532. DOI: 10.1137/23M155147X.
- [Gil08] M. B. Giles. “Multilevel Monte Carlo Path Simulation”. In: *Operations Research* 56.3 (2008), pp. 607–617. DOI: 10.1287/opre.1070.0496.
- [GL94] J. Gaines and T. Lyons. “Random Generation of Stochastic Area Integrals”. In: *SIAM Journal on Applied Mathematics* 54.4 (1994), pp. 1132–1146.
- [GL97] J. Gaines and T. Lyons. “Variable step size control in the numerical solution of stochastic differential equations”. In: *SIAM Journal on Applied Mathematics* 57.5 (1997), pp. 1455–1484.
- [Hab21] K. Habermann. “A semicircle law and decorrelation phenomena for iterated Kolmogorov loops”. In: *Journal of the London Mathematical Society* 103.2 (2021), pp. 558–586. DOI: <https://doi.org/10.1112/jlms.12384>. URL: <https://londmathsoc.onlinelibrary.wiley.com/doi/abs/10.1112/jlms.12384>.
- [HJ19] M. Hefter and A. Jentzen. “On arbitrarily slow convergence rates for strong numerical approximations of Cox-Ingersoll-Ross processes and squared Bessel processes”. In: *Finance and Stochastics* 23 (Jan. 2019). DOI: 10.1007/s00780-018-0375-5.
- [HK21] D. Higham and P. Kloeden. *An Introduction to the Numerical Simulation of Stochastic Differential Equations*. Other Titles in Applied Mathematics. Society for Industrial and Applied Mathematics, 2021. ISBN: 9781611976434. URL: <https://books.google.co.uk/books?id=b9wXEAAAQBAJ>.
- [HNW08] E. Hairer, S. Nørsett, and G. Wanner. *Solving Ordinary Differential Equations I Nonstiff Problems*. Second Revised Edition. Berlin: Springer, 2008.
- [HNW93] E. Hairer, S. Norsett, and G. Wanner. *Solving Ordinary Differential Equations I: Nonstiff Problems*. Vol. 8. Springer Berlin Heidelberg, Jan. 1993. ISBN: 978-3-540-56670-0. DOI: 10.1007/978-3-540-78862-1.
- [HW02] E. Hairer and G. Wanner. *Solving Ordinary Differential Equations II Stiff and Differential-Algebraic Problems*. Second Revised Edition. Berlin: Springer, 2002.
- [IJE15] S. Ilie, K. R. Jackson, and W. H. Enright. “Adaptive Time-Stepping for the Strong Numerical Solution of Stochastic Differential Equations”. In: *Numer. Algorithms* 68.4 (2015), pp. 791–812. DOI: <https://doi.org/10.1007/s11075-014-9872-6>.
- [Jel+23] A. Jelinčič et al. *Generative Modelling of Lévy Area for High Order SDE Simulation*. 2023. arXiv: 2308.02452 [stat.ML].
- [JOA19] P. E. Jacob, J. O’Leary, and Y. F. Atchadé. *Unbiased Markov chain Monte Carlo with couplings*. 2019. arXiv: 1708.03625 [stat.ME].
- [Kid+21a] P. Kidger et al. “Efficient and Accurate Gradients for Neural SDEs”. In: *Advances in Neural Information Processing Systems*. Ed. by M. Ranzato et al. Vol. 34. Curran Associates, Inc., 2021, pp. 18747–18761. URL: https://proceedings.neurips.cc/paper_files/paper/2021/file/9ba196c7a6e89eafd0954de80fc1b224-Paper.pdf.
- [Kid+21b] P. Kidger et al. “Neural SDEs as Infinite-Dimensional GANs”. In: *Proceedings of the 38th International Conference on Machine Learning*. Ed. by M. Meila and T. Zhang. Vol. 139. Proceedings of Machine Learning Research. PMLR, July 2021, pp. 5453–5463. URL: <https://proceedings.mlr.press/v139/kidger21b.html>.
- [KPW92] P. Kloeden, E. Platen, and I. Wright. “The approximation of multiple stochastic integrals”. In: *Stochastic Analysis and Applications* 10.4 (1992), pp. 431–441.

- [LG97] D. S. Lemons and A. Gythiel. “Paul Langevin’s 1908 paper “On the Theory of Brownian Motion” [“Sur la théorie du mouvement brownien,” C. R. Acad. Sci. (Paris) 146, 530–533 (1908)]”. In: *American Journal of Physics* 65.11 (Nov. 1997), pp. 1079–1081.
- [Li+19] X. Li et al. “Stochastic Runge-Kutta Accelerates Langevin Monte Carlo and Beyond”. In: *Advances in Neural Information Processing Systems*. Ed. by H. Wallach et al. Vol. 32. Curran Associates, Inc., 2019. URL: https://proceedings.neurips.cc/paper_files/paper/2019/file/7d265aa7147bd3913fb84c7963a209d1-Paper.pdf.
- [Li+20] X. Li et al. “Scalable Gradients and Variational Inference for Stochastic Differential Equations”. In: *Proceedings of The 2nd Symposium on Advances in Approximate Bayesian Inference*. Ed. by C. Zhang et al. Vol. 118. Proceedings of Machine Learning Research. PMLR, Dec. 2020, pp. 1–28. URL: <https://proceedings.mlr.press/v118/li20a.html>.
- [Mau98] S. Mauthner. “Step size control in the numerical solution of stochastic differential equations”. In: *Journal of Computational and Applied Mathematics* 100.1 (1998), pp. 93–109. ISSN: 0377-0427. DOI: [https://doi.org/10.1016/S0377-0427\(98\)00139-3](https://doi.org/10.1016/S0377-0427(98)00139-3). URL: <https://www.sciencedirect.com/science/article/pii/S0377042798001393>.
- [MR22] J. Mrongowius and A. Röbler. “On the approximation and simulation of iterated stochastic integrals and the corresponding Lévy areas in terms of a multidimensional Brownian motion”. In: *Stochastic Analysis and Applications* 40.3 (2022), pp. 397–425.
- [Nea03] R. M. Neal. “Slice Sampling”. In: *The Annals of Statistics* 31.3 (2003), pp. 705–741. ISSN: 00905364.
- [RN17] C. Rackauckas and Q. Nie. “Adaptive methods for stochastic differential equations via natural embeddings and rejection sampling with memory”. In: *Discrete and continuous dynamical systems. Series B* 22 7 (2017), pp. 2731–2761.
- [RöB10] A. Röbler. “Runge–Kutta Methods for the Strong Approximation of Solutions of Stochastic Differential Equations”. In: *SIAM Journal on Numerical Analysis* 48.3 (2010), pp. 922–952. DOI: [10.1137/09076636X](https://doi.org/10.1137/09076636X).
- [RV23] L. Riou-Durand and J. Vogrinc. *Metropolis Adjusted Langevin Trajectories: a robust alternative to Hamiltonian Monte Carlo*. 2023. arXiv: 2202.13230 [stat.CO].
- [Sal+11] J. K. Salmon et al. “Parallel random numbers: as easy as 1, 2, 3.” In: *Proc. High Performance Computing, Networking, Storage and Analysis* (2011), pp. 1–12.
- [Söd02] G. Söderlind. “Automatic Control and Adaptive Time-Stepping”. In: *Numerical Algorithms* 31 (Jan. 2002), pp. 281–310. DOI: [10.1023/A:1021160023092](https://doi.org/10.1023/A:1021160023092).
- [Söd03] G. Söderlind. “Digital Filters in Adaptive Time-Stepping”. In: *ACM Transactions on Mathematical Software* 20.1 (2003), pp. 1–26.
- [Son+21] Y. Song et al. “Score-Based Generative Modeling through Stochastic Differential Equations”. In: *International Conference on Learning Representations*. 2021. URL: <https://openreview.net/forum?id=PXTIG12RRHS>.
- [SZ21] J. M. Sanz-Serna and K. C. Zygalakis. “Wasserstein distance estimates for the distributions of numerical approximations to ergodic stochastic differential equations”. In: *Journal of Machine Learning Research* 22.242 (2021), pp. 1–37. URL: <http://jmlr.org/papers/v22/21-0453.html>.
- [Wik01] M. Wiktorsson. “Joint characteristic function and simultaneous simulation of iterated Itô integrals for multiple independent Brownian motions”. In: *The Annals of Applied Probability* 11.2 (2001), pp. 470–487.

A Updated bridge and final_interpolation functions

Algorithm 4 Updated bridge, based on theorems 3.4 and 3.5.

Input: l - depth in tree, s - start of the interval, $\bar{Y}_s, \bar{Y}_u, \bar{Y}_{s,u}$ - BM and Lévy areas, $\hat{\rho}$ - PRNG seed

if $Y = (W, H)$ **then**

for $x \in \{s, u, [s, u]\}$ **let** $(W_x, \bar{H}_x) \leftarrow \bar{Y}_x$

$\hat{\rho}_1, \hat{\rho}_2 \leftarrow \text{split_seed}(\hat{\rho}, 2)$

$Z \leftarrow \mathcal{N}(0, \frac{1}{16}(u-s)\mathbf{I}_d, \hat{\rho}_1)$

$N \leftarrow \mathcal{N}(0, \frac{1}{12}(u-s)\mathbf{I}_d, \hat{\rho}_2)$

$W_{s,t} \leftarrow \frac{1}{2}W_{s,u} + \frac{3}{2(u-s)}\bar{H}_{s,u} + Z, \quad W_{t,u} \leftarrow \frac{1}{2}W_{s,u} - \frac{3}{2(u-s)}\bar{H}_{s,u} - Z$

$\bar{H}_{s,t} \leftarrow \frac{1}{8}\bar{H}_{s,u} - \frac{u-s}{4}Z + \frac{u-s}{4}N, \quad \bar{H}_{t,u} \leftarrow \frac{1}{8}\bar{H}_{s,u} - \frac{u-s}{4}Z - \frac{u-s}{4}N$

$W_t \leftarrow W_s + W_{s,t}$

$\bar{H}_t \leftarrow \bar{H}_s + \bar{H}_{s,t} + \frac{1}{2}(tW_s - sW_t)$

for $x \in \{t, [s, t], [t, u]\}$ **let** $\bar{Y}_x \leftarrow (W_x, \bar{H}_x)$

else

▷ in this case $Y = (W, H, K)$

for $x \in \{s, u, [s, u]\}$ **let** $(W_x, \bar{H}_x, \bar{K}_x) \leftarrow \bar{Y}_x$

$\hat{\rho}_1, \hat{\rho}_2, \hat{\rho}_3 \leftarrow \text{split_seed}(\hat{\rho}, 3)$

$Z \leftarrow \mathcal{N}(0, \frac{1}{16}(u-s)\mathbf{I}_d, \hat{\rho}_1)$

$X_1 \leftarrow \mathcal{N}(0, \frac{1}{768}(u-s)\mathbf{I}_d, \hat{\rho}_2)$

$X_2 \leftarrow \mathcal{N}(0, \frac{1}{2880}(u-s)\mathbf{I}_d, \hat{\rho}_3)$

$W_{s,t} \leftarrow \frac{1}{2}W_{s,u} + \frac{3}{2(u-s)}\bar{H}_{s,u} + Z, \quad W_{t,u} \leftarrow \frac{1}{2}W_{s,u} - \frac{3}{2(u-s)}\bar{H}_{s,u} - Z$

$\bar{H}_{s,t} \leftarrow \frac{1}{8}\bar{H}_{s,u} + \frac{15}{8(u-s)}\bar{K}_{s,u} - \frac{u-s}{4}Z + \frac{u-s}{2}X_1, \quad \bar{H}_{t,u} \leftarrow \frac{1}{8}\bar{H}_{s,u} - \frac{15}{8(u-s)}\bar{K}_{s,u} - \frac{u-s}{4}Z - \frac{u-s}{2}X_1$

$\bar{K}_{s,t} \leftarrow \frac{1}{32}\bar{K}_{s,u} - \frac{(u-s)^2}{8}X_1 + \frac{(u-s)^2}{4}X_2, \quad \bar{K}_{t,u} \leftarrow \frac{1}{32}\bar{K}_{s,u} - \frac{(u-s)^2}{8}X_1 - \frac{(u-s)^2}{4}X_2$

$W_t \leftarrow W_s + W_{s,t}$

$B_s^{0,t} \leftarrow W_s - \frac{s}{t}W_t$

$\bar{H}_t \leftarrow \bar{H}_s + \bar{H}_{s,t} + \frac{t}{2}B_s^{0,t}$

$\bar{K}_t \leftarrow \bar{K}_s + \bar{K}_{s,t} + \frac{t-s}{2}\bar{H}_s - \frac{s}{2}\bar{H}_{s,t} + \frac{(t-s)^2 - s^2}{12}B_s^{0,t}$

for $x \in \{t, [s, t], [t, u]\}$ **let** $\bar{Y}_x \leftarrow (W_x, \bar{H}_x, \bar{K}_x)$

end if

return $\bar{Y}_t, \bar{Y}_{s,t}, \bar{Y}_{t,u}$

Algorithm 5 Updated final_interpolation, based on theorems 3.6 and 3.7.

Input: s - start time, r - target time, u - end time, $\bar{Y}_s, \bar{Y}_u, \bar{Y}_{s,u}$ - BM and Lévy areas, $\hat{\rho}$ - PRNG seed

if $Y = (W, H)$ **then**

for $x \in \{s, u, [s, u]\}$ **let** $(W_x, \bar{H}_x) \leftarrow \bar{Y}_x$

$\hat{\rho}_1, \hat{\rho}_2 \leftarrow \text{split_seed}(\hat{\rho}, 2)$

$X_1 \leftarrow \mathcal{N}(0, \mathbf{I}_d, \hat{\rho}_1)$

$X_2 \leftarrow \mathcal{N}(0, \mathbf{I}_d, \hat{\rho}_2)$

$a \leftarrow \frac{(r-s)^{\frac{7}{2}}(u-r)^{\frac{1}{2}}}{2(u-s)\sqrt{(r-s)^3+(u-r)^3}}$

$b \leftarrow \frac{(r-s)^{\frac{1}{2}}(u-r)^{\frac{7}{2}}}{2(u-s)\sqrt{(r-s)^3+(u-r)^3}}$

$c \leftarrow \frac{\sqrt{3}(r-s)^{\frac{3}{2}}(u-r)^{\frac{3}{2}}}{6\sqrt{(r-s)^3+(u-r)^3}}$

$W_{s,r} \leftarrow \frac{r-s}{u-s}W_{s,u} + 6\frac{(r-s)(u-r)}{(u-r)^3}\bar{H}_{s,u} + 2\frac{a+b}{u-s}X_1$

$\bar{H}_{s,r} \leftarrow \left(\frac{r-s}{u-s}\right)^3\bar{H}_{s,u} - aX_1 + cX_2$

$W_r \leftarrow W_s + W_{s,r}$

$\bar{H}_r \leftarrow \bar{H}_s + \bar{H}_{s,r} + \frac{1}{2}(rW_s - sW_r)$

$\bar{Y}_r \leftarrow (W_r, \bar{H}_r)$

else

▷ in this case $Y = (W, H, K)$

for $x \in \{s, u, [s, u]\}$ **let** $(W_x, \bar{H}_x, \bar{K}_x) \leftarrow \bar{Y}_x$

$H_{s,u} \leftarrow \frac{1}{u-s}\bar{H}_{s,u}$ $K_{s,u} \leftarrow \frac{1}{(u-s)^2}\bar{K}_{s,u}$

$\tilde{W}_{s,r} \leftarrow \frac{r-s}{u-s}W_{s,u} + 6\frac{(r-s)(u-r)}{(u-s)^2}H_{s,u} + 120\frac{(r-s)(u-r)(\frac{u+s}{2}-r)}{(u-s)^3}K_{s,u}$

$\tilde{H}_{s,r} \leftarrow \frac{(r-s)^2}{(u-s)^2}H_{s,u} + 30\frac{(r-s)^2(u-r)}{(u-s)^3}K_{s,u}$

$\tilde{K}_{s,r} \leftarrow \frac{(r-s)^3}{(u-s)^3}K_{s,u}$

$(\hat{W}_{s,r}, \hat{H}_{s,r}, \hat{K}_{s,r}) \leftarrow \mathcal{N}(0, \Sigma_r, \hat{\rho})$ where Σ_r is as in equation 7

$W_{s,r} \leftarrow \tilde{W}_{s,r} + \hat{W}_{s,r}$

$\bar{H}_{s,r} \leftarrow (r-s)(\tilde{H}_{s,r} + \hat{H}_{s,r})$

$\bar{K}_{s,r} \leftarrow (r-s)^2(\tilde{K}_{s,r} + \hat{K}_{s,r})$

$W_r \leftarrow W_s + W_{s,r}$

$B_s^{0,r} \leftarrow W_s - \frac{s}{r}W_r$

$\bar{H}_r \leftarrow \bar{H}_s + \bar{H}_{s,r} + \frac{r}{2}B_s^{0,r}$

$\bar{K}_r \leftarrow \bar{K}_s + \bar{K}_{s,r} + \frac{r-s}{2}\bar{H}_s - \frac{s}{2}\bar{H}_{s,r} + \frac{(r-s)^2-s^2}{12}B_s^{0,r}$

$\bar{Y}_r \leftarrow (W_r, \bar{H}_r, \bar{K}_r)$

end if

return \bar{Y}_r

B Proofs of results from Section 3

B.1 Proof of Chen's relation for (W, H, K)

Theorem 3.3 (Chen's relation). *For times $0 \leq s < t < u$, Chen's relation is given by*

$$\begin{aligned} W_{s,u} &= W_{s,t} + W_{t,u}, \\ \bar{H}_{s,u} &= \bar{H}_{s,t} + \bar{H}_{t,u} + \frac{u-s}{2} B_t^{s,u}, \\ \bar{K}_{s,u} &= \bar{K}_{s,t} + \bar{K}_{t,u} + \frac{u-t}{2} \bar{H}_{s,t} - \frac{t-s}{2} \bar{H}_{t,u} + \frac{(u-t)^2 - (t-s)^2}{12} B_t^{s,u}. \end{aligned} \tag{3}$$

where $B_t^{s,u} := W_{s,t} - \frac{t-s}{u-s} W_{s,u}$ denotes the Brownian bridge associated with W on $[s, u]$.

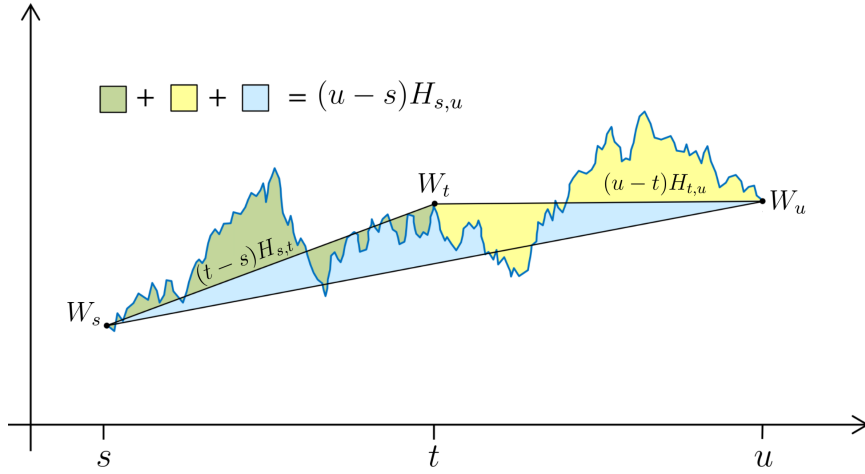


Figure 5: Chen's relation for space-time Lévy area (from [Fos20]).

Proof. The relation for \bar{H} appears in [Fos20] and can be easily deduced using figure 5. We will derive the identity for \bar{K} , which is new here.

Let $0 \leq s < t < u$ be some times. Recall Eq. (14):

$$\begin{aligned} B_r^{s,t} &= B_r^{s,u} - \frac{r-s}{t-s} B_t^{s,u} \quad \text{for } r \in [s, t] \\ B_r^{t,u} &= B_r^{s,u} - \frac{u-r}{u-t} B_t^{s,u} \quad \text{for } r \in [t, u]. \end{aligned}$$

Substituting this into the definition of $\bar{K}_{s,u} = \int_s^u B_r^{s,u} \left(\frac{u+s}{2} - r \right) dr$ gives

$$\begin{aligned}
\bar{K}_{s,t} + \bar{K}_{t,u} &= \int_s^t B_r^{s,t} \left(\frac{t+s}{2} - r \right) dr + \int_s^t B_r^{t,u} \left(\frac{u+t}{2} - r \right) dr \\
&= \int_s^u B_r^{s,u} \left(\frac{u+s}{2} - r \right) dr - \int_s^t B_r^{s,t} \frac{u-t}{2} dr + \int_s^t \left(-\frac{r-s}{t-s} B_t^{s,u} \right) \left(\frac{u+s}{2} - r \right) dr \\
&\quad + \int_t^u B_r^{t,u} \frac{t-s}{2} dr - \int_t^u \left(-\frac{u-r}{u-t} B_t^{s,u} \right) \left(\frac{u+s}{2} - r \right) dr \\
&= \bar{K}_{s,u} - \frac{u-t}{2} (t-s) H_{s,t} - \frac{1}{12} (t-s)(s+3u-4t) B_t^{s,u} \\
&\quad + \frac{t-s}{2} (u-t) H_{t,u} - \frac{1}{12} (u-t)(3s+u-4t) B_t^{s,u} \\
&= \bar{K}_{s,u} - \frac{u-t}{2} \bar{H}_{s,t} + \frac{t-s}{2} \bar{H}_{t,u} - \frac{(u-t)^2 - (t-s)^2}{12} B_t^{s,u}
\end{aligned}$$

as required. \square

B.2 Proof of the Midpoint update rule for (W, H, K)

Theorem 3.5 (Midpoint Brownian bridge for (W, H, K)). *Let t denote the midpoint $t = s + \frac{1}{2}(u-s)$. Then,*

$$\begin{aligned}
W_{s,t} &= \frac{1}{2} W_{s,u} + \frac{3}{2} H_{s,u} + Z & W_{t,u} &= \frac{1}{2} W_{s,u} - \frac{3}{2} H_{s,u} - Z, \\
H_{s,t} &= \frac{1}{4} H_{s,u} + \frac{15}{4} K_{s,u} - \frac{1}{2} Z + X_1, & H_{t,u} &= \frac{1}{4} H_{s,u} - \frac{15}{4} K_{s,u} - \frac{1}{2} Z - X_1, \\
K_{s,t} &= \frac{1}{8} K_{s,u} - \frac{1}{2} X_1 + X_2, & K_{t,u} &= \frac{1}{8} K_{s,u} - \frac{1}{2} X_1 - X_2,
\end{aligned}$$

where $W_{s,u}, H_{s,u}, K_{s,u}, Z, X_1, X_2$ are independent Gaussian random variables with

$$Z \sim \mathcal{N}\left(0, \frac{u-s}{16}\right), \quad X_1 \sim \mathcal{N}\left(0, \frac{u-s}{768}\right), \quad X_2 \sim \mathcal{N}\left(0, \frac{u-s}{2880}\right).$$

Proof. We will prove this as a special case of Theorem 3.7, in which we set $r = t = \frac{s+u}{2}$ to obtain

$$\begin{aligned}
\mathbb{E}[W_{s,t}|Y_{s,u}] &= \frac{1}{2} W_{s,u} + \frac{3}{2} H_{s,u}, \\
\mathbb{E}[H_{s,t}|Y_{s,u}] &= \frac{1}{4} H_{s,u} + \frac{15}{4} K_{s,u}, \\
\mathbb{E}[K_{s,t}|Y_{s,u}] &= \frac{1}{8} K_{s,u},
\end{aligned}
\quad \Sigma_t = (u-s) \begin{bmatrix} \frac{1}{16} & -\frac{1}{32} & 0 \\ -\frac{1}{32} & \frac{13}{768} & -\frac{1}{1536} \\ 0 & -\frac{1}{1536} & \frac{31}{46080} \end{bmatrix}. \quad (11)$$

The Cholesky decomposition $\Sigma_t = LL^T$ gives

$$L = \sqrt{(u-s)} \begin{bmatrix} \frac{1}{4} & 0 & 0 \\ -\frac{1}{8} & \frac{1}{\sqrt{768}} & 0 \\ 0 & -\frac{1}{\sqrt{3072}} & \frac{1}{\sqrt{2880}} \end{bmatrix}. \quad (12)$$

Combining equations (11) and (12) gives precisely the desired values of $W_{s,t}, H_{s,t}$ and $K_{s,t}$. We then obtain $W_{t,u}, H_{t,u}$ and $K_{t,u}$ via Chen's relation. \square

An alternative proof can be found on page 144 of [Fos20].

B.3 Proof of the general Brownian bridge for (W, H, K)

Theorem 3.7 (General Brownian bridge for (W, H, K)). *For any $0 \leq s < u$ and $r \in [s, u]$ the distribution of $Y_{s,r}$ conditioned on $Y_{s,u}$ is Gaussian with the following mean:*

$$\begin{aligned}\mathbb{E}[W_{s,r}|Y_{s,u}] &= \frac{r-s}{u-s}W_{s,u} + 6\frac{(r-s)(u-r)}{(u-s)^2}H_{s,u} + 120\frac{(r-s)(u-r)(\frac{1}{2}(u+s)-r)}{(u-s)^3}K_{s,u}, \\ \mathbb{E}[H_{s,r}|Y_{s,u}] &= \frac{(r-s)^2}{(u-s)^2}H_{s,u} + 30\frac{(r-s)^2(u-r)}{(u-s)^3}K_{s,u}, \\ \mathbb{E}[K_{s,r}|Y_{s,u}] &= \frac{(r-s)^3}{(u-s)^3}K_{s,u},\end{aligned}\tag{6}$$

and the following covariance matrix:

$$\Sigma_r := \mathbb{E}\left[(Y_{s,r} - \mathbb{E}[Y_{s,r}|Y_{s,u}]) (Y_{s,r} - \mathbb{E}[Y_{s,r}|Y_{s,u}])^T \mid Y_{s,u}\right] = \begin{bmatrix} \Sigma_r^{WW} & \Sigma_r^{WH} & \Sigma_r^{WK} \\ \Sigma_r^{WH} & \Sigma_r^{HH} & \Sigma_r^{HK} \\ \Sigma_r^{WK} & \Sigma_r^{HK} & \Sigma_r^{KK} \end{bmatrix},\tag{7}$$

with coefficients

$$\begin{aligned}\Sigma_r^{WW} &= \frac{(r-s)(u-r)\left((2r-u-s)^4 + 4(r-s)^2(u-r)^2\right)}{(u-s)^5}, \\ \Sigma_r^{WH} &= -\frac{(r-s)^3(u-r)\left((r-s)^2 - 3(r-s)(u-r) + 6(u-r)^2\right)}{2(u-s)^5}, \\ \Sigma_r^{WK} &= \frac{(r-s)^4(u-r)(2r-u-s)}{12(u-s)^5}, \\ \Sigma_r^{HH} &= \frac{r-s}{12}\left(1 - \frac{(r-s)^3\left((r-s)^2 + 2(r-s)(u-r) + 16(u-r)^2\right)}{(u-s)^5}\right), \\ \Sigma_r^{HK} &= -\frac{(r-s)^5(u-r)}{24(u-s)^5}, \quad \Sigma_r^{KK} = \frac{r-s}{720}\left(1 - \frac{(r-s)^5}{(u-s)^5}\right).\end{aligned}$$

Proof. Fix $0 \leq s < u$ and let $r \in [s, u]$. Since the vectors $Y_{s,r}$ and $Y_{s,u}$ are jointly Gaussian, we can decompose $Y_{s,r}$ into

$$Y_{s,r} = \tilde{Y}_{s,r} + \hat{Y}_{s,r},$$

where $\hat{Y}_{s,r}$ is a zero-mean Gaussian vector independent of $Y_{s,u}$, and $\tilde{Y}_{s,r} = \mathbb{E}[Y_{s,r}|Y_{s,u}]$ is a deterministic function of $Y_{s,u}$. To compute $\tilde{Y}_{s,r}$, we use the Brownian polynomial from [FLO20]:

$$\tilde{W}_{s,r} := \mathbb{E}[W_{s,r}|Y_{s,u}] = \frac{r-s}{u-s}W_{s,u} + 6\frac{(r-s)(u-r)}{(u-s)^2}H_{s,u} + 120\frac{(r-s)(u-r)(\frac{u+s}{2}-r)}{(u-s)^3}K_{s,u}.\tag{13}$$

Recall that the Brownian bridge is defined as $B_r^{s,u} := W_{s,r} - \frac{r-s}{u-s}W_{s,u}$ with the convention that $B_s^{s,s} := 0$. Rearranging gives the following identities:

$$\begin{aligned}B_q^{s,r} &= B_q^{s,u} - \frac{q-s}{r-s}B_r^{s,u} \quad \text{for } q \in [s, r], \\ B_q^{r,u} &= B_q^{s,u} - \frac{u-q}{u-r}B_r^{s,u} \quad \text{for } q \in [r, u].\end{aligned}\tag{14}$$

We can use Eq. (13) to compute

$$\begin{aligned}\tilde{B}_r^{s,u} &:= \mathbb{E}[B_r^{s,u}|Y_{s,u}] = \tilde{W}_{s,r} - \frac{r-s}{u-s}\tilde{W}_{s,u} \\ &= \frac{(r-s)(u-r)}{(u-s)^2} (6H_{s,u} + 60K_{s,u}) - 120\frac{(r-s)^2(u-r)}{(u-s)^3}K_{s,u},\end{aligned}$$

which, when combined with Eq. (14), gives

$$\begin{aligned}\tilde{B}_q^{s,r} &:= \mathbb{E}[B_q^{s,r}|Y_{s,u}] \\ &= \frac{(q-s)(r-q)}{(u-s)^2} (6H_{s,u} + 60K_{s,u}) + 120\frac{(q-s)((u-r)(r-s) - (u-q)(q-s))}{(u-s)^3}K_{s,u}.\end{aligned}$$

Substituting this into the definition of $H_{s,r}$ and $K_{s,r}$, we obtain a formula for $\tilde{Y}_{s,r}$:

$$\begin{aligned}\tilde{W}_{s,r} &= \frac{r-s}{u-s}W_{s,u} + 6\frac{(r-s)(u-r)}{(u-s)^2}H_{s,u} + 120\frac{(r-s)(u-r)(\frac{u+s}{2}-r)}{(u-s)^3}K_{s,u}, \\ \tilde{H}_{s,r} &:= \mathbb{E}[H_{s,r}|Y_{s,u}] = \frac{1}{r-s}\int_s^r \tilde{B}_q^{s,r} dq \\ &= \frac{(r-s)^2}{(u-s)^2}H_{s,u} + 30\frac{(r-s)^2(u-r)}{(u-s)^3}K_{s,u}, \\ \tilde{K}_{s,r} &:= \mathbb{E}[K_{s,r}|Y_{s,u}] = \frac{1}{(r-s)^2}\int_s^r \tilde{B}_q^{s,r} \left(\frac{r+s}{2}-q\right) dq \\ &= \frac{(r-s)^3}{(u-s)^3}K_{s,u}.\end{aligned}\tag{15}$$

All that remains is to compute the covariance matrix of $\hat{Y}_{s,r}$, which depends only on s, r , and u . Since $(Y_{s,r})_{r \geq s}$ is a Gaussian process, we have

$$\Sigma_r := \mathbb{E}[\hat{Y}_{s,r}\hat{Y}_{s,r}^T] = \mathbb{E}[Y_{s,r}Y_{s,r}^T] - \mathbb{E}[\tilde{Y}_{s,r}\tilde{Y}_{s,r}^T].\tag{16}$$

By construction $W_{s,r}, H_{s,r}$, and $K_{s,r}$ are independent (see [Fos20] for details). Hence $\mathbb{E}[Y_{s,r}Y_{s,r}^T]$ is diagonal with the following entries

$$\text{var}(W_{s,r}) = r-s, \quad \text{var}(H_{s,r}) = \frac{r-s}{12}, \quad \text{var}(K_{s,r}) = \frac{r-s}{720}.\tag{17}$$

To compute the matrix $\mathbb{E}[\tilde{Y}_{s,r}\tilde{Y}_{s,r}^T]$ we can just multiply each line of Eq. (15) with each other and then use the independence of $W_{s,u}, H_{s,u}$ and $K_{s,u}$.

Taking the difference $\mathbb{E}[Y_{s,r}Y_{s,r}^T] - \mathbb{E}[\tilde{Y}_{s,r}\tilde{Y}_{s,r}^T]$ gives the desired coefficients. \square